THE ASTROPHYSICAL JOURNAL, 372:132–160, 1991 May 1

VLA AND VLBI ANGULAR BROADENING MEASUREMENTS: THE DISTRIBUTION OF INTERSTELLAR SCATTERING AT LOW GALACTIC LATITUDES

A. L. FEY[1]
University of Iowa; and Naval Research Laboratory, Code 4033.2FE, Center for Advanced Space Sensing, Washington, DC 20375

S. R. SPANGLER
Department of Physics and Astronomy, Van Allen Hall, University of Iowa, Iowa City, IA 52242

AND

J. M. CORDES
Astronomy Department, Space Science Building, Cornell University, Ithaca, NY 14853
Received 1990 April 25; accepted 1990 October 15

ABSTRACT

We report dual-frequency VLA and multifrequency VLBI angular broadening measurements of a number of radio sources located along the Galactic plane in the longitude range $l = 20°$–$80°$ and with Galactic latitude $|b| < 0.°5$. We use the λ^2 dependence of scattered angular size to distinguish between intrinsic and scattered source structure. Our observations support a previous report that the structure of the extragalactic source 1849+005 is dominated by interstellar scattering. This source appears to be one of the most heavily scattered sources known. We have also observed angular broadening for the sources 1855+031 and 2008+33D. Five additional sources, 1905+079, 1922+155, 1932+204, 1954+282, and 2001+304 show indications of being affected by interstellar scattering. For the remaining sources we obtain upper limits to scattering with the value of the upper limit depending on the observed source structure. We find that the observed scattering in the Galactic plane decreases with increasing Galactic longitude, reaching a minimum at $l \approx 60°$ and then becoming prominent again in the Cygnus region. The magnitude of scattering in the interarm region between $l = 50°$–$70°$ is comparable to that predicted by a model calculation of a "smooth" component of interstellar turbulence. The more intense "clumps" of interstellar turbulence may therefore be mainly confined to the spiral arms of the Galaxy. A computer simulation was undertaken to find clump properties consistent with our observations. This simulation indicates that a complex distribution of clumps is necessary, with a range of scattering strengths, and that the form of the clump distribution as well as the density of clumps must change with increasing galactocentric distance. The simulation constrains the z scale height in the Cygnus region to be ~40–70 pc. Although there is a weak correlation between scattering and H166α emission measure, interpretation of this result is unclear and leaves open the identification of the regions of enhanced turbulence.

Subject headings: interstellar: matter — radio sources: general — turbulence

1. INTRODUCTION

In light of recent observations (Dennison et al. 1984; Cordes, Weisberg, & Boriakoff 1985; Alurkar, Slee, & Bobra 1986; Cordes et al. 1988; Fey, Spangler, & Mutel 1989) it now seems evident that electron density turbulence in the interstellar medium consists of two components, a "smooth" component with uniform Galactic distribution and a more intense "clumped" component. The clumped component is confined mainly to the Galactic plane and has a scale height characteristic of Population I objects (e.g., H II regions, supernova remnants, etc.). We are largely ignorant of many important characteristics of both types of turbulence but especially the sites of the clumped component. Although Molnar et al. (1991) have tentatively identified the scattering of Cyg X-3 with the H II region DR 11 and Moran et al. (1990) suggest that the H II region NGC 6334A is responsible for the scattering of the radio source NGC 6334B, most observational attempts to associate enhanced scattering with any particular phase of the interstellar medium have been unsuccessful. From angular broadening measurements, Fey, Spangler, & Mutel (1989) reported enhanced scattering in the direction of the Cygnus "superbubble" (Bochkarev & Sitnik 1985). Although the scattering is clearly associated with the Cygnus region, Fey, Spangler, & Mutel (1989) were unable to link the enhanced scattering with any particular astronomical object. Spangler et al. (1986) reported 610, 1663, and 4991 MHz VLBI angular broadening measurements of five extragalactic sources whose lines of sight pass near supernova remnants. Although broadening was definitely seen for two of the sources, the authors could not unambiguously attribute the scattering material to the associated supernova remnant.

One of the sources observed by Spangler et al. (1986) was 1849+005. The line of sight to this source passes within 8′ of the supernova remnant G33.6+0.1. The authors failed to detect this source in any experiment and concluded that if their null result was due to scattering, the implied 1 GHz broadening size was in excess of 350 mas. Dennison et al. (1984) also failed to detect this source in a 408 MHz very long baseline interferometry (VLBI) experiment. Frail & Clifton (1989) report observations of a highly scattered pulsar within 10′ of 1849+005. The amount of scattering in this region, as determined from the pulsar pulse broadening measurement, is consistent with that implied by the null result of Spangler et al. (1986). Since these results imply broadening sizes accessible to the National Radio Astronomy Observatory (NRAO)[2] Very

[1] National Research Council/NRL Cooperative Research Associate.

[2] The NRAO is operated by Associated Universities, Inc., under cooperative agreement with the National Science Foundation.

Large Array (VLA), we undertook VLA observations to obtain angular broadening measurements of 1849+005 and a number of other sources in the Galactic plane. We also undertook a series of VLBI observations of additional Galactic plane sources.

VLA observations provide significant advantages over VLBI observations: increased sensitivity, better calibration, and a greater number of antennas. The VLA is sensitive to angular scales of several tenths of an arcsecond at 1.4 GHz ($\sim 2''$ synthesized beam in A array) and can thus detect broadened sources that would be resolved to the point of nondetection with VLBI. VLBI, on the other hand, is sensitive to angular scales of a few milliarcseconds at 1.6 GHz and thus allows us to probe scattering of sources that would appear pointlike to the VLA. The two instruments have different sensitivities to scattering and thus allow us to probe scattering over a wide range of angular sizes.

Since we are searching for scattering, we desire extragalactic objects. Although pulsars are generally superior to extragalactic objects in scattering studies, angular broadening of extragalactic objects is easily interpreted and can be observed with standard interferometers. The bulk of previous scattering observations in the Galaxy have been made mostly by pulsar pulse broadening and decorrelation bandwidth measurements (Cordes, Weisberg, & Boriakoff 1985; Alurkar, Slee, & Bobra 1986). The angular sampling of pulsar observations is limited by the distribution of pulsars on the sky, whereas for angular broadening measurements the high surface density of extragalactic objects ensures that many probe sources may be found for any particular region of the sky. Furthermore, a given line of sight to an extragalactic object passes through the entire disk of the Galaxy, whereas for a pulsar the scattering screen is distance dependent. Thus more scattering occurs for extragalactic objects, the scattering screen is not dependent on the distance to the object, and many probe sources can be found.

In addition to investigating the scattering of 1849+005, the observations also provided the opportunity to map the scattering material in the Galactic plane. The main purpose of our observations was to investigate the dependence of angular broadening on Galactic latitude and longitude so that we could attempt to associate specific astronomical objects with the "clumped" component of interstellar turbulence. Our angular broadening observations in the Galactic plane probe scattering through the whole of the Galaxy and can be reliably compared along close lines of sight.

In §§ 2 and 3 we describe the VLA observations and their results, respectively. We discuss the VLBI observations and results in §§ 4 and 5. Scattering information is extracted from the results of all the observations in § 6 and summarized in § 7. We discuss the results in terms of a "smooth" component of interstellar turbulence and compare our results with the Galactic plane distribution of H166α recombination line emission. Finally, in § 8 we discuss a computer simulation intended to investigate the properties of the more intense "clumped" component of interstellar turbulence.

2. VLA OBSERVATIONS

We made 333 and 1465 MHz observations of 40 Galactic plane radio sources using the VLA. Dual-frequency observations were undertaken so as to use the λ^2 dependence of scattered angular size in identifying scattering. Our source list was taken from a preliminary version of a 1.5 GHz VLA snapshot continuum survey of the Galactic plane by Garwood et al. (1988). Sources were chosen such that they were within $\approx 10°$ of the source 1849+005 and had a 1.5 GHz survey peak flux density greater than 50 mJy. Table 1 lists the sources observed. Column (1) lists the source name. Columns (2) and (3) give the equatorial coordinates (epoch 1950), and columns (4) and (5) list the Galactic longitude and latitude, respectively. Column (6) lists comments for each source.

Observations were made over an 11 hr period on 1987 August 20–21 while the VLA was in the "A" configuration. Each program source was observed for a single 2 minute scan at both 333 and 1465 MHz. The source 1849+005 was observed during several scans over a number of different hour angles for a total observing time of 20 minutes at both 333 and 1465 MHz. We also observed 1849+005 for a single one minute scan at 4860 MHz. Data at 1465 and 4860 MHz were taken in two adjacent 50 MHz bandpasses. Data at 333 MHz were taken in a single 2 MHz IF bandpass. The source 3C 286 served as an absolute flux density calibrator at each frequency. The flux density of 3C 286 was assumed to be 26.77 Jy at 333 MHz, 14.51 Jy at 1465 MHz, and 7.41 Jy at 4860 MHz (Baars et al. 1977). The flux density value for 3C 286 at 333 MHz is an extrapolation just outside the range of applicability of the spectral parameters given by Baars et al. (1977). The sources 1938−155 and 1821+107 were monitored frequently as secondary amplitude and phase calibrators. At the time of the observations, 18 of the 27 VLA antennas were equipped with 333 MHz receivers. Of these, 13 produced usable data at this frequency.

The calibrated visibility data for each program source were edited and mapped using the NRAO Astronomical Image Processing System (AIPS) software. Inspection of the 1465 and 333 MHz data revealed that at short spacings the data were dominated by bright extended emission. Continuum emission at low longitudes in the Galactic plane is dominated by large-scale distributed emission which is not well sampled by the VLA in the "A" configuration. Use of the shortest spacings will produce poor dynamic range images because of the presence of this extended emission. Furthermore, because it is poorly sampled, the extended emission cannot be adequately CLEANed. Therefore, to increase the dynamic range in our images, a minimum (u, v) spacing was specified in the mapping algorithm. Restricting the minimum spacing is valid since, for a scattering survey, we are primarily interested in compact emission. Minimum spacings of 10^4 λ and 2000 λ were used in the mapping of the 1465 MHz data and the 333 MHz data, respectively. Our observations are therefore insensitive to angular scales larger than $\sim 15''$ at 1465 MHz and $70''$ at 333 MHz. Extended emission did not appear to be a problem at 4860 MHz.

After mapping, the images were CLEANed in the standard manner. The full width at half-maximum of the Gaussian restoring beams for the images are $\sim 0''.5$, $1''.4$, and $8''$ at 4860, 1465, and 333 MHz, respectively. Two-dimensional elliptical Gaussian models were fitted to those images which showed structurally simple emission to obtain estimates of the source brightness and angular size. Because of the limited amount and quality of the data we list only the mean angular sizes (geometric mean of the major and minor axes) of the fitted models. We have not attempted to measure anisotropy of the scattering disks.

3. VLA OBSERVATIONAL RESULTS

In this section we describe the results of our VLA observations. Of the 40 sources listed in Table 1, 31 were detected at 1465 MHz. The nine sources not detected at 1465 MHz appear

TABLE 1

GALACTIC PLANE SOURCES OBSERVED WITH THE VLA

Source (1)	R.A.(1950) (2)	Decl.(1950) (3)	l (4)	b (5)	Notes (6)
1832−081.....	$18^h32^m30^s.722$	−8°09′51″.41	23°.861	−0°.125	a,b,c,d
1831−080.....	18 31 54.065	−8 02 36.89	23.898	0.065	a,b,c,d
1831−07B.....	18 31 16.882	−7 56 48.19	23.912	0.246	a
1831−079.....	18 31 42.430	−7 57 05.69	23.957	0.150	a,b,c,d
1832−078.....	18 32 05.873	−7 49 07.70	24.121	0.127	b,d,e,f,g
1834−076.....	18 34 04.162	−7 38 15.18	24.507	−0.222	a,b,c,d
1834−067.....	18 34 49.008	−6 43 57.40	25.395	0.033	a,d
1835−068.....	18 35 26.748	−6 48 40.39	25.397	−0.142	a,b,c,d,g
1835−065.....	18 35 27.725	−6 34 46.34	25.605	−0.038	b,e,f,g
1835−063.....	18 35 23.659	−6 21 49.97	25.788	0.077	a,b,c,g
1835−061.....	18 35 21.503	−6 06 04.07	26.017	0.207	b,c,e,g
1835−060.....	18 35 20.061	−6 05 06.11	26.029	0.220	b,e,f,g
1836−061.....	18 36 26.081	−6 09 26.50	26.091	−0.057	a,d,g
1836−060.....	18 36 47.635	−6 02 15.78	26.239	−0.080	b,e,f,g
1842−033.....	18 42 15.725	−3 23 38.40	29.212	−0.068	a,b,c,d,g
1844−021.....	18 44 23.143	−2 10 43.50	30.535	0.021	a,b,c,d,g
1845−014.....	18 45 36.492	−1 29 51.76	31.280	0.063	a,b,c,d
1849+000.....	18 49 34.416	0 04 32.52	33.133	−0.092	a,b,c,d,g
1849+005.....	18 49 13.573	0 31 53.34	33.498	0.195	b,e,f,h
1850+007.....	18 50 17.503	0 51 45.61	33.914	0.110	a,b,c,d,g
1850+011.....	18 50 47.486	1 10 52.61	34.255	0.146	a,d,g
1850+01B.....	18 50 45.960	1 11 12.34	34.257	0.154	a,b,c,d,g
1851+012.....	18 51 41.768	1 15 27.29	34.427	−0.020	b,e,f
1852+016.....	18 52 39.065	1 37 26.47	34.862	−0.063	a,b,c,g
1852+021.....	18 52 44.119	2 06 56.31	35.308	0.145	b,e,f,h
1853+022.....	18 53 02.954	2 15 15.91	35.467	0.139	a,b,c
1854+02B.....	18 54 38.961	2 39 08.17	36.004	−0.032	b,e,f
1854+026.....	18 54 45.266	2 38 24.98	36.006	−0.061	b,e,f,g
1855+031.....	18 55 32.157	3 09 10.59	36.551	0.002	b,e,f,g,h,i
1858+050.....	18 58 39.430	5 00 04.25	38.550	0.164	a,g
1858+05B.....	18 58 30.678	5 04 06.42	38.593	0.228	b,e,f,g,h
1901+058.....	19 01 16.098	5 48 26.83	39.565	−0.040	b,e,f,g,h
1902+067.....	19 02 55.108	6 47 34.03	40.629	0.054	b,e,f,g,i
1904+078.....	19 04 50.580	7 48 00.32	41.742	0.097	a,b,c
1905+079.....	19 05 12.001	7 56 45.32	41.912	0.087	b,e,f,g,h
1906+083.....	19 06 04.483	8 20 37.26	42.365	0.080	b,e,f,g,h
1908+087.....	19 08 03.326	8 47 24.00	42.988	−0.146	a,f,g,h,j
1907+09B.....	19 07 46.994	9 00 16.92	43.147	0.014	a,d,g
1907+090.....	19 07 58.253	9 00 07.78	43.166	−0.028	a,d,g
1908+090.....	19 08 09.874	9 03 24.66	43.237	−0.045	a,g

[a] Position from R. W. Garwood, private communication.
[b] Detected with VLA at 1.46 GHz.
[c] Diffuse or extended emission on VLA maps.
[d] Identified by Garwood et al. 1988 to be within 2′.4 of a recombination line source.
[e] Position from 1.46 GHz VLA maps, this paper.
[f] Structurally simple emission on VLA maps.
[g] Observed with MK II VLBI.
[h] Detected with VLA at 0.33 GHz.
[i] VLBI fringes found.
[j] Not listed in Garwood et al. 1988.

to be heavily resolved to the VLA at this frequency in the "B" array observations of Garwood et al. (1988). It is possible that these sources were completely resolved by our higher resolution "A" array observations. Of the 31 sources detected at 1465 MHz, seven were also detected at 333 MHz. One additional source (1908+087) was detected only at 333 MHz. Sixteen of the 32 detected sources exhibit structurally simple emission while the remaining 16 sources show diffuse or extended emission. We also note that 17 of the observed sources have been identified by Garwood et al. (1988) to have positions within 2′.4 of a recombination line source. This information is listed in column (6) of Table 1. Column (6) also indicates the survey sources that were observed using Mk II VLBI. Of the 27 sources listed in this table that were observed with a VLB interferometer, only two were detected. These and additional VLBI observations are discussed in the next section.

Figures 1–4 show contour plots of our VLA images for each source detected at each frequency, with the exception of three images. The data for 1831−079 and 1835−068 at 1465 MHz and 1906+083 at 333 MHz produced poor-quality maps that could not be CLEANed properly. Inspection of Figures 1–4 reveals that the sources fall into at least two distinct categories, those with complex extended emission (Fig. 1) and those with structurely simple or compact emission (Figs. 2, 3, and 4). Sources that fall in the first category, such as 1834−076, 1844−021, and 1849+000, show distributed, asymmetric source structure and are probably pieces of H II regions or supernova remnants. Many of the extended sources can be

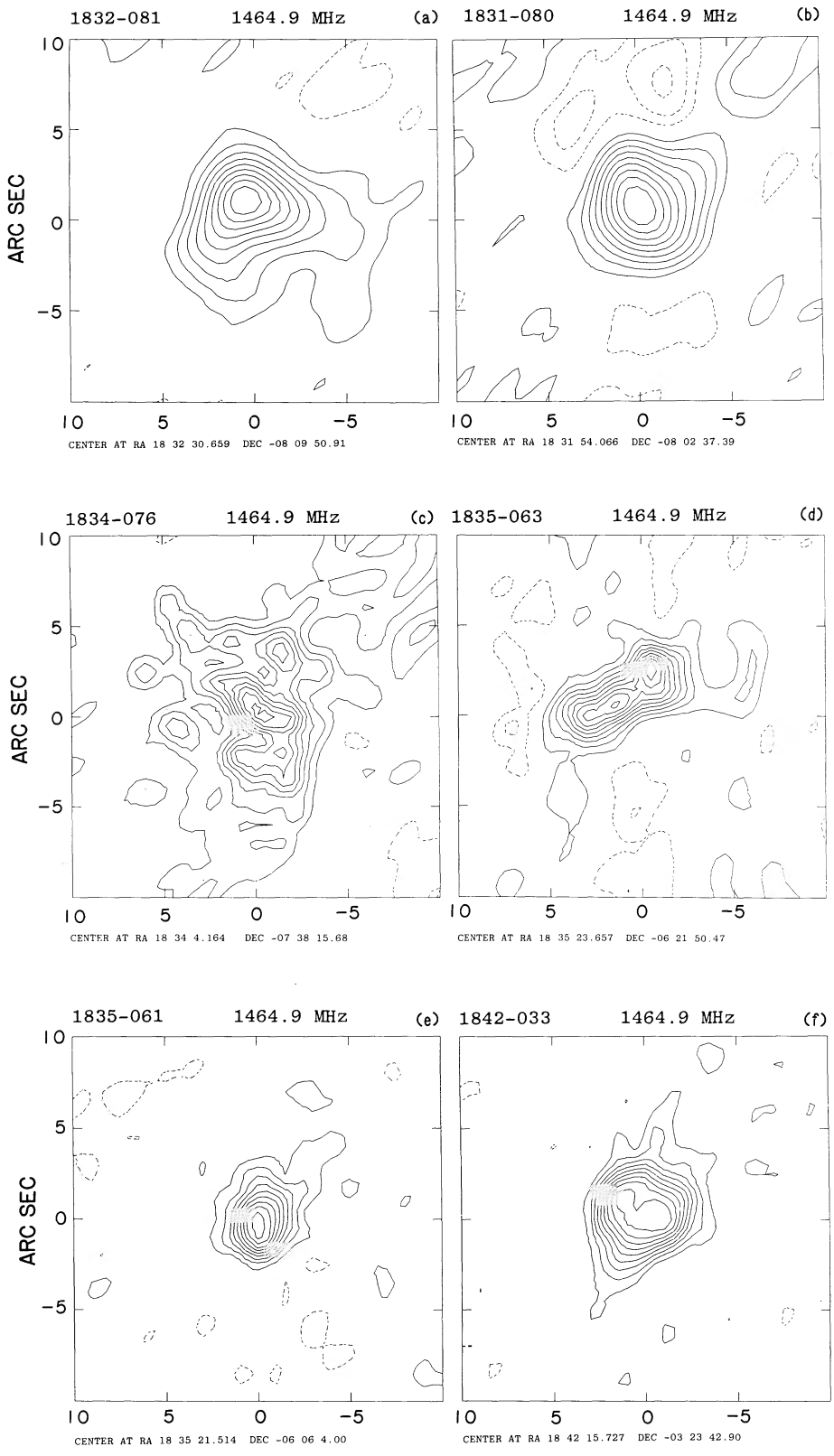

FIG. 1.—VLA images of extended sources detected only at 1465 MHz. Contours are at −90, −80, −70, −60, −50, −40, −30, −20, −10, −5, 10, 20, 30, 40, 50, 60, 70, 80, and 90% of the peak intensities which are (*a*) 0.021, (*b*) 0.022, (*c*) 0.013, (*d*) 0.020, (*e*) 0.015, (*f*) 0.016, (*g*) 0.026, (*h*) 0.010, (*i*) 0.025, (*j*) 0.023, (*k*) 0.031, (*l*) 0.010, (*m*) 0.017, and (*n*) 0.016 Jy beam^{-1}. The angular resolution in each panel is 1.″4 with the exception of (*a*) and (*b*) which is 3″. These sources are not used for scattering estimates.

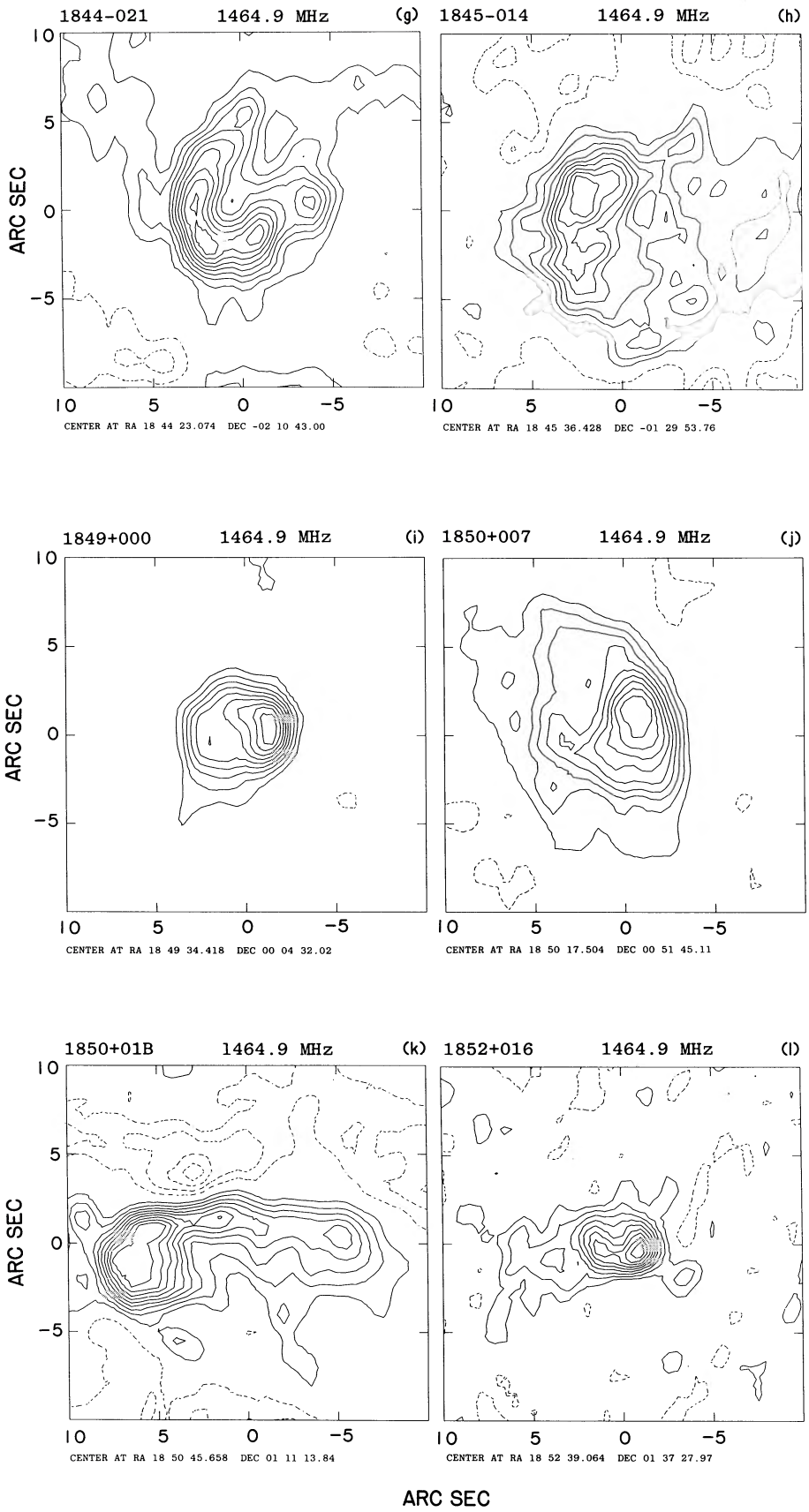

FIG. 1—*Continued*

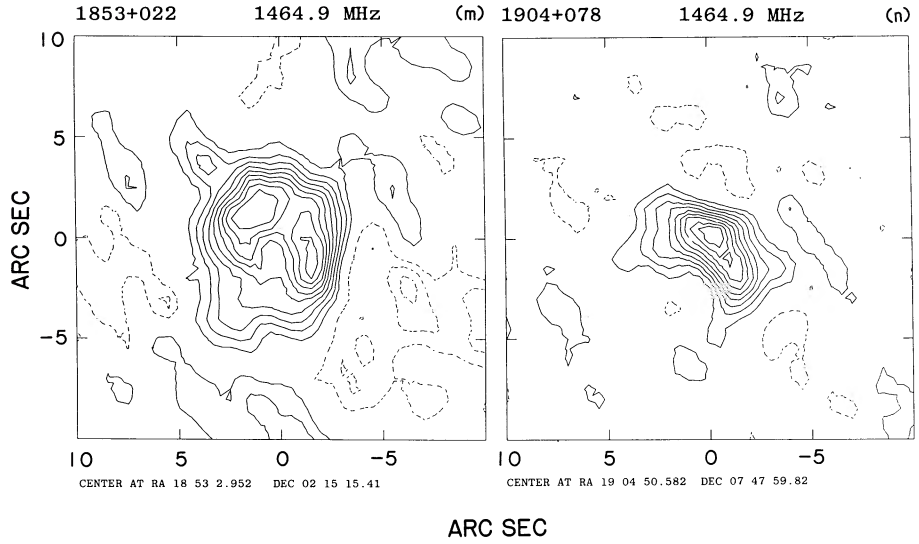

FIG. 1—*Continued*

associated with regions of apparently Galactic emission on the 5 GHz continuum maps of Altenhoff et al. (1978). We include images of extended sources for comparison and as examples of sources which were excluded from our analysis. They are also included for the benefit of anyone who may wish to make further observations of these sources.

A sample useful for our purposes was formed from those sources which show structurally simple emission, as opposed to diffuse or extended emission, and lie well away from extended continuum emission on the 5 GHz maps of Altenhoff et al. (1978). Listed in Table 2 are the single-component Gaussian models fitted to the images of the 16 sources which have these characteristics. Column (1) gives the source name, and column (2) lists the frequency of observation. The results of the model fitting are contained in columns (3) and (4) which list, respectively, the integrated flux density and angular size in arcseconds. Angular diameters are geometric mean values of the major and minor axes of the two-dimensional elliptical Gaussian models fitted to the images at each of the observing frequencies. In most cases the quoted errors on angular size are derived from models using two different fitting windows, one larger than the other. The angular size errors for the remaining few sources were determined by the maximum and minimum values calculated by the AIPS fitting routine JMFIT.

TABLE 2

GAUSSIAN MODEL FITS TO GALACTIC PLANE VLA SOURCES

Source (1)	Frequency (GHz) (2)	Flux Density (Jy) (3)	Angular Size FWHM (4)
1832−078.....	1.465	0.101	2″.01 ± 0″.29
1835−065.....	1.465	0.293	0.84 ± 0.03
1835−060.....	1.465	0.053	1.44 ± 0.10
1836−060.....	1.465	0.064	1.65 ± 0.03
1849+005.....	0.333	1.879	7.13 ± 0.23
	1.465	0.634	0.56 ± 0.08
	4.860	0.593	0.10 ± 0.03
1851+012.....	1.465	0.073	1.48 ± 0.06
1852+021.....	0.333	0.197	≤3.45
	1.465	0.113	0.74 ± 0.09
1854+02B.....	1.465	0.044	≤1.01
1854+026.....	1.465	0.056	≤0.48
1855+031.....	0.333	1.288	1.46 ± 0.16
	1.465	0.993	≤0.67
1858+05B.....	0.333	0.201	≤4.14
	1.465	0.099	0.91 ± 0.03
1901+058.....	0.333	1.583	1.61 ± 0.21
	1.465	0.532	0.39 ± 0.10
1902+067.....	1.465	0.107	≤0.32
1905+079.....	0.333	0.194	4.31 ± 0.49
	1.465	0.081	0.36 ± 0.06
1906+083.....	1.465	0.096	0.99 ± 0.12
1908+087.....	0.333	0.351	5.77 ± 0.29

Examination of Table 2 reveals that over half the sources listed were detected at only a single frequency, thereby providing no information on frequency dependence of angular size. Consequently, these sources can be used only to place upper limits on any scattering contribution to the observed angular size. However, examination of a plot of the measured 1465 MHz angular sizes listed in Table 2 versus Galactic longitude revealed a tendency for the sources inside of 30° longitude to have angular sizes in excess of those outside of 30°. Sources inside of 30° are heavily resolved by the VLA and show smooth brightness distributions with no indication of intrinsic structure, thus suggesting that scattering rather than intrinsic structure might dominate their observed properties. With the resolution of these observations, we would have expected to see some intrinsic structure if these are Galactic objects. Our interpretation is that for sources inside of 30° longitude the observed size is dominated by interstellar scattering, whereas for higher longitudes the measured sizes are a combination of intrinsic and scattered structure. Indeed, several of the sources with multifrequency detections, outside of 30° longitude, have angular sizes which do not show a λ^2 dependence.

Only 1849+005, 1855+031, and possibly 1905+079 show clear evidence of being affected by interstellar scattering as demonstrated by a λ^2 dependence of angular size. The source 1849+005 has an angular size which scales roughly as the square of the wavelength. The images of this source are shown in Figure 4 and reveal the simple structure characteristic of a broadened image. The structure of the source 1855+031 appears to be dominated by interstellar scattering. Our VLA images for this source are shown in Figures 3*c* and 3*d*. As can be seen from these figures, this source shows no structure at

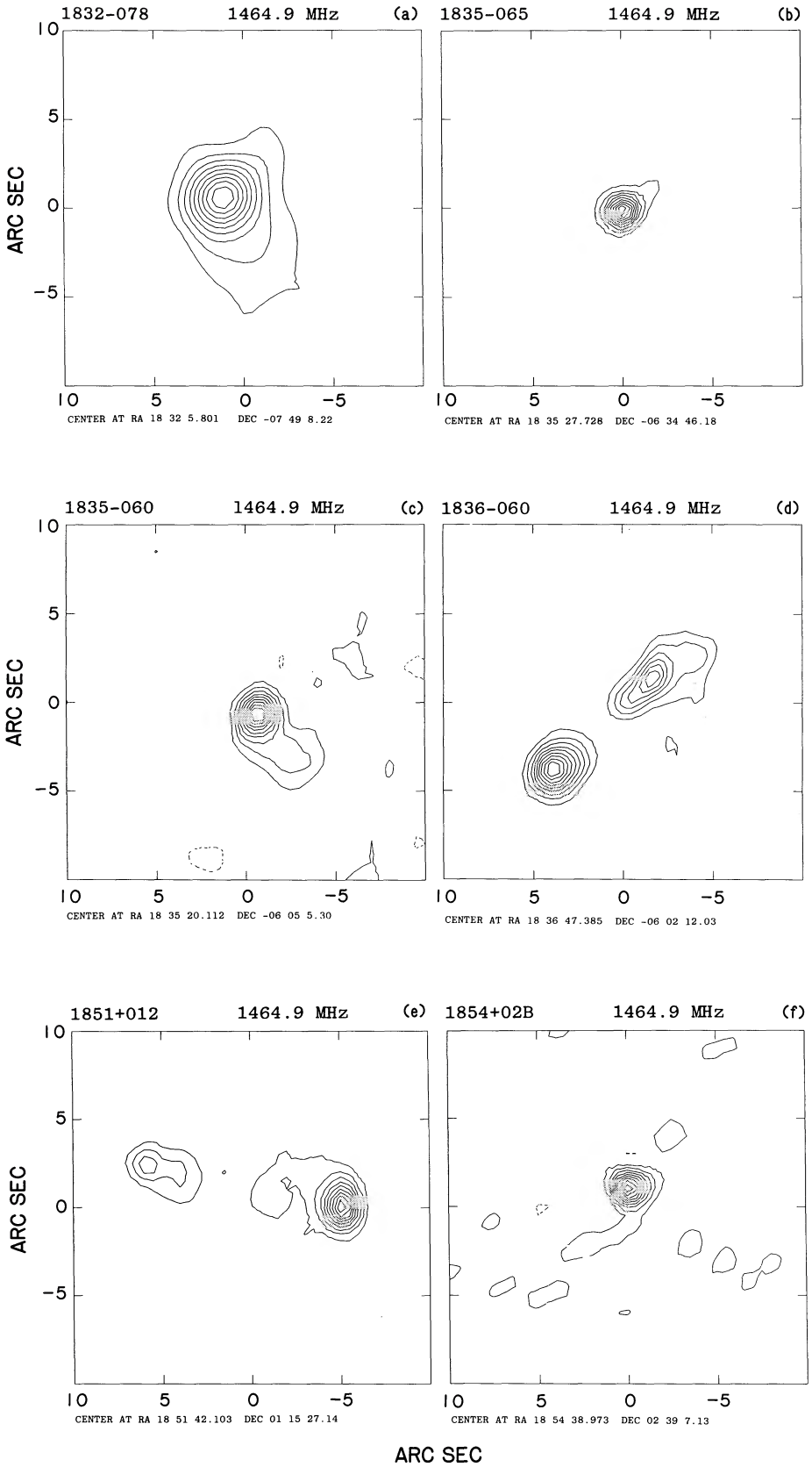

FIG. 2.—VLA images of compact sources detected at a single frequency. Contours are at −90, −80, −70, −60, −50, −40, −30, −20, −10, −5, 10, 20, 30, 40, 50, 60, 70, 80, and 90% of the peak intensities which are (*a*) 0.071, (*b*) 0.200, (*c*) 0.025, (*d*) 0.028, (*e*) 0.037, (*f*) 0.035, (*g*) 0.053, (*h*) 0.092, (*i*) 0.062, and (*j*) 0.236 Jy beam^{-1}. The angular resolution in each panel is 1.″4 with the exception of (*a*) which is 3″ and (*j*) which is 8″.

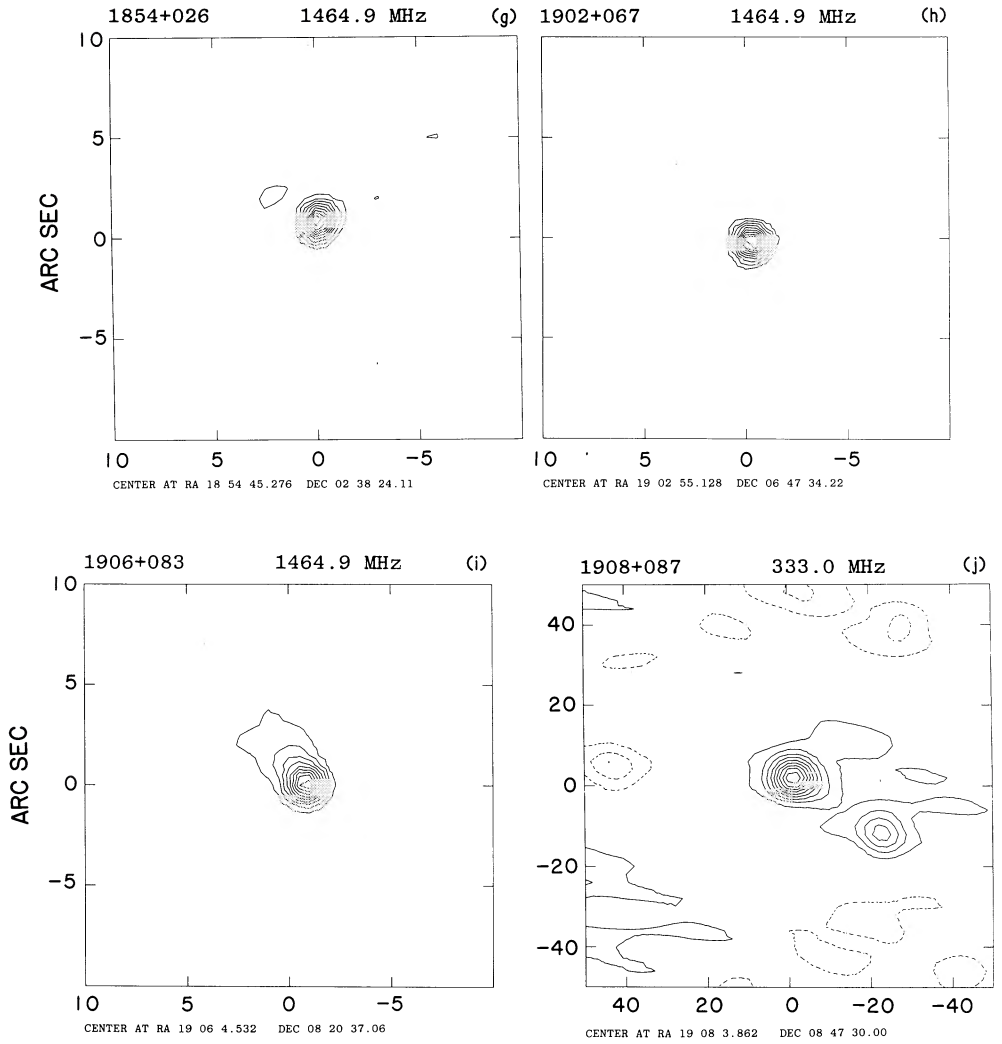

FIG. 2—*Continued*

VLA resolution. Since this source is unresolved at 1465 MHz, the measurements listed in Table 2 alone do not indicate the presence of angular broadening. However, this source was also detected with a VLB interferometer at both 1.66 and 4.99 GHz. The results of our VLBI observations, which will be discussed in a later section, confirm the scattered nature of this source. Our VLA images of 1905+079 (Figs. 3*i* and 3*j*) show smooth brightness distributions with no evidence for intrinsic structure. In addition, the source has an angular size which scales roughly as the square of the wavelength. However, our data are insufficient to rule out a contribution to the angular size from intrinsic structure. Consequently, we use 1905+079 only to set an upper limit to scattering.

We make a final comment on the significance of the fact that eight of the sources listed in Table 2 were detected only at 1465 MHz. One possibility for the nondetections at 333 MHz is the weakness of the sources and the relative insensitivity of the VLA for Galactic plane observations. Due to interference in the bandpass it was necessary to make the 333 MHz observations in VLA spectral line mode. The resultant effective bandwidth of 2 MHz thus decreased the sensitivity of the 333 MHz observations by a factor of ~ 5 over that of the 1465 MHz observations. Furthermore, at 333 MHz, antenna sensitivity is decreased and system temperature increased over that at 1465 MHz. The net effect of these two system characteristics is that some sources might not have been detected due to low signal-to-noise ratio. The other, more interesting, possibility is that these sources are so heavily broadened that they are completely resolved at 333 MHz. In the presence of scattering, a source with an angular diameter of 1″ at 1465 MHz would be broadened to $\approx 20''$ at 333 MHz. The visibility of a 20″ source drops to 50% at a baseline length of $\approx 4500\lambda$. As mentioned above, a minimum spacing of 2000λ was specified in the mapping of the 333 MHz data. With the VLA in the "A" configuration, the visibility of a source with an angular diameter this large or larger would not be well sampled. As can be seen in Table 2, four of the sources detected only at 1465 MHz have angular sizes larger than 1″. Thus, if scattering dominates their observed structure, we would not expect these sources to have been detected at 333 MHz.

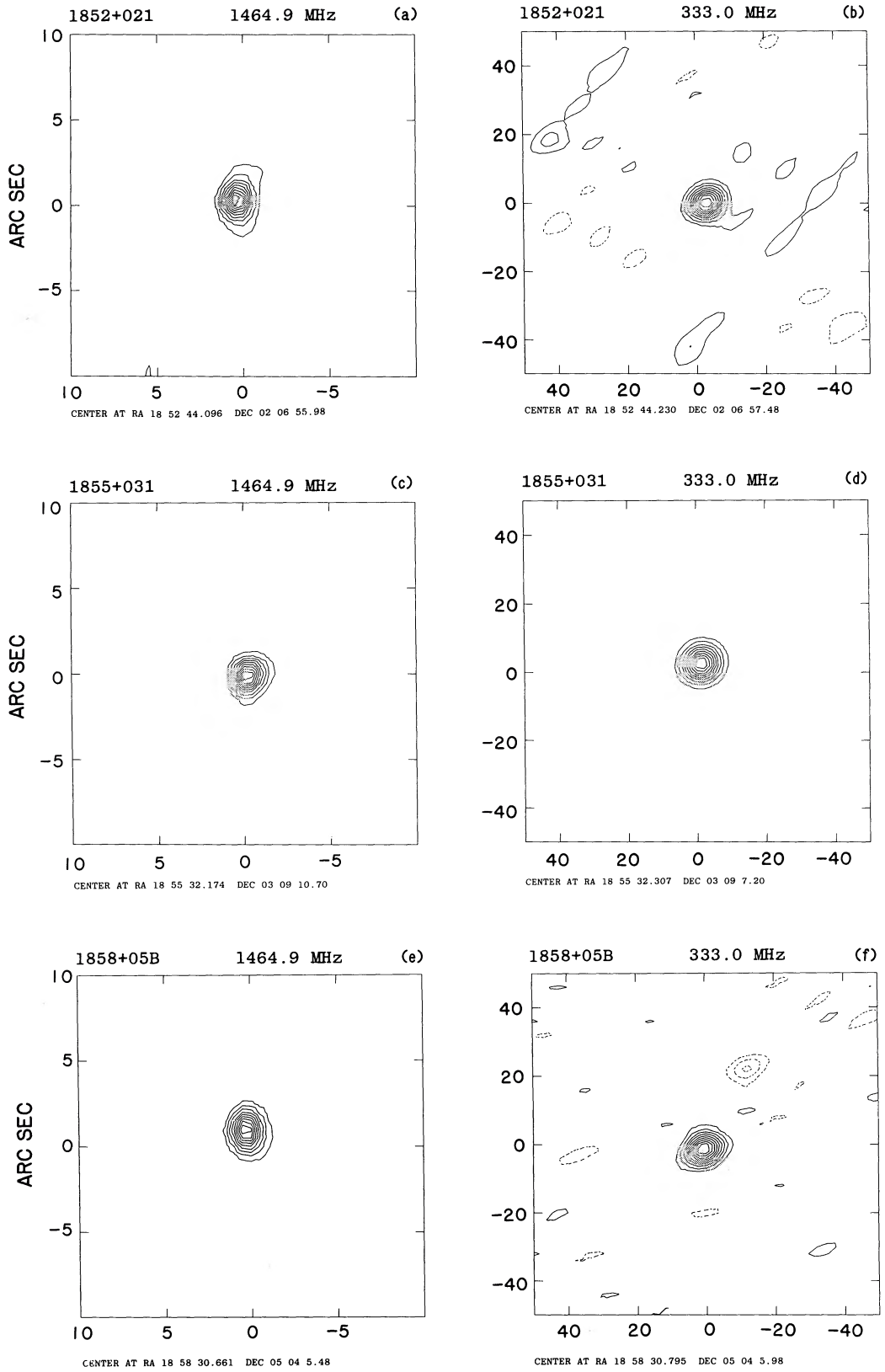

FIG. 3.—VLA images of compact sources detected at both 1465 MHz and 333 MHz. Contours are at −90, −80, −70, −60, −50, −40, −30, −20, −10, −5, 10, 20, 30, 40, 50, 60, 70, 80, and 90% of the peak intensities which are (*a*) 0.083, (*b*) 0.202, (*c*) 0.822, (*d*) 1.165, (*e*) 0.063, (*f*) 0.200, (*g*) 0.293, (*h*) 1.397, (*i*) 0.066, and (*j*) 0.146 Jy beam^{-1}. The angular resolution in each panel is 1.″4 for the 1465 MHz images and 8″ for the 333 MHz images.

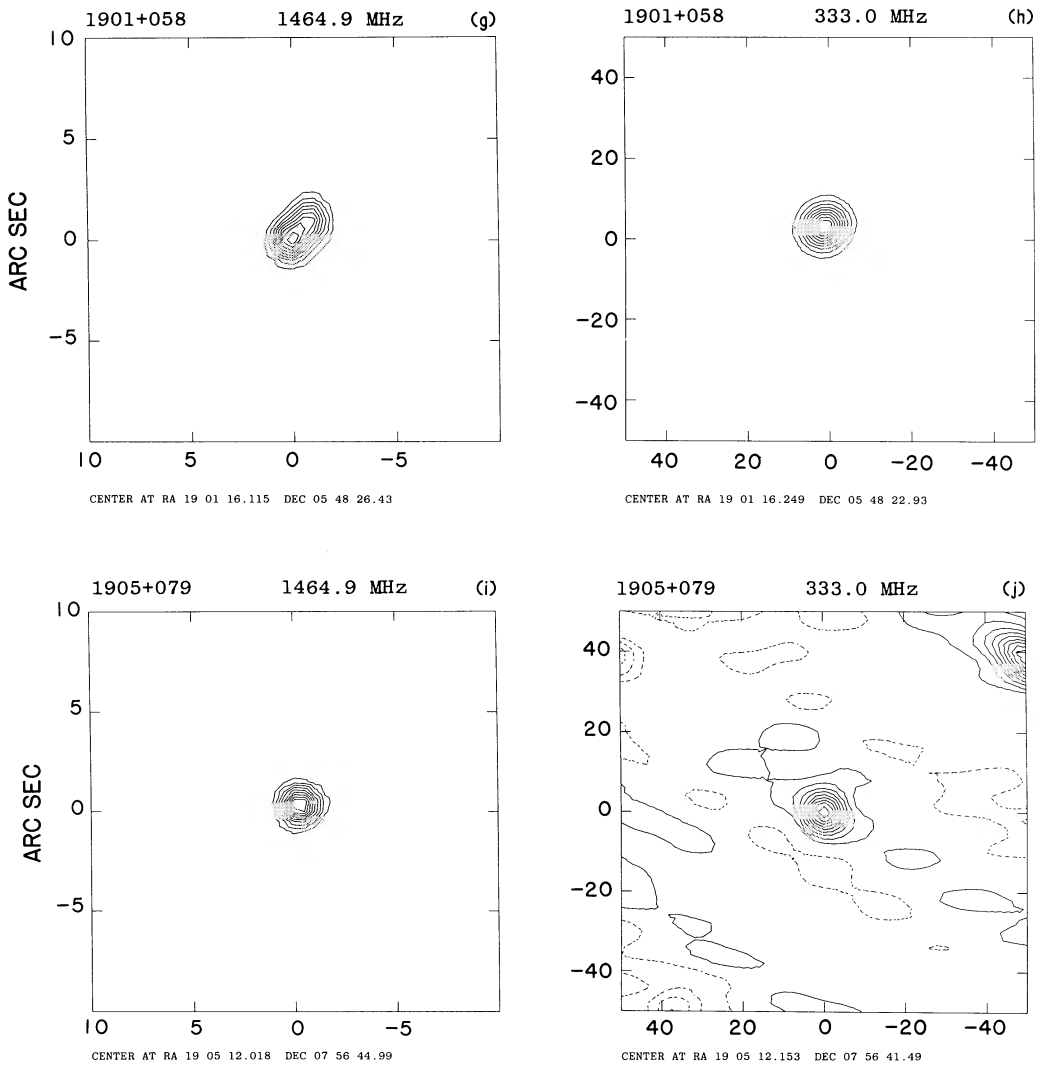

FIG. 3—*Continued*

4. VLBI OBSERVATIONS

We made observations of 62 Galactic plane sources at frequencies of 1.66 and 4.99 GHz and nine sources at 0.61 GHz using the Mk II VLBI recording system. Multifrequency observations were undertaken so that we could use the λ^2 dependence of angular broadening to distinguish between scattered and intrinsic source structure. The source list, which is again taken from the preliminary version of the survey by Garwood et al. (1988), is given in Table 3. Additional sources observed with VLBI are included in Table 1 as indicated by the notes in column (6). The sources chosen had a 1.5 GHz peak flux density $S_\nu \geq 50$ mJy, which is about the detection limit of Mk II VLBI, and lie in the longitude range $l = 24°$–$80°$.

The 4.99 GHz observations were carried out in 1987 May using antennas at Effelsberg, West Germany (BONN); Bologna, Italy (BOLOGNA); Westford, Massachusetts (HSTK); Green Bank, West Virginia (NRAO); Fort Davis, Texas (FDVS); Big Pine, California (OVRO); Berkeley, California (HCRK); and Socorro, New Mexico (VLA in phased array mode). The 1.66 GHz VLB observations were made in 1987 March using antennas at NRAO, VLA (phased array mode), HCRK, HSTK, FDVS, OVRO, BONN, BOLOGNA, Ottawa, Ontario (ARO); North Liberty, Iowa (IOWA); and Arecibo, Puerto Rico (ARECIBO). Finally, 0.61 GHz observations were carried out in 1988 June using an interferometer consisting of BONN, NRAO, IOWA, FDVS, OVRO, ARECIBO, Jodrell Bank, England (JODRELL); and Westerbork, The Netherlands (WSRT). The observations at 1.66 and 4.99 GHz were made using a single 15 minute scan for each source. Only those sources which showed fringes at 1.66 and 4.99 GHz were observed at 0.61 GHz. Thus, the 0.61 GHz observations were made using 15 minute scans over a number of different hour angles. The data we present are therefore rather rudimentary, and can yield only simple information on source structure. The compact double source 2050+364 was monitored frequently at 1.66 and 4.99 GHz as an aid in the amplitude calibration at these frequencies. The (assumed) unresolved source 0235+164 was observed at 0.61 GHz as an amplitude calibrator for the 0.61 GHz data. The videotapes were correlated with the CIT/JPL Block II correlator at the California Institute of Technology.

The correlated data were processed with the NRAO Astronomical Image Processing System (AIPS) global fringe-fitting software. Fringe-fitting intervals of 3 minutes were used. After

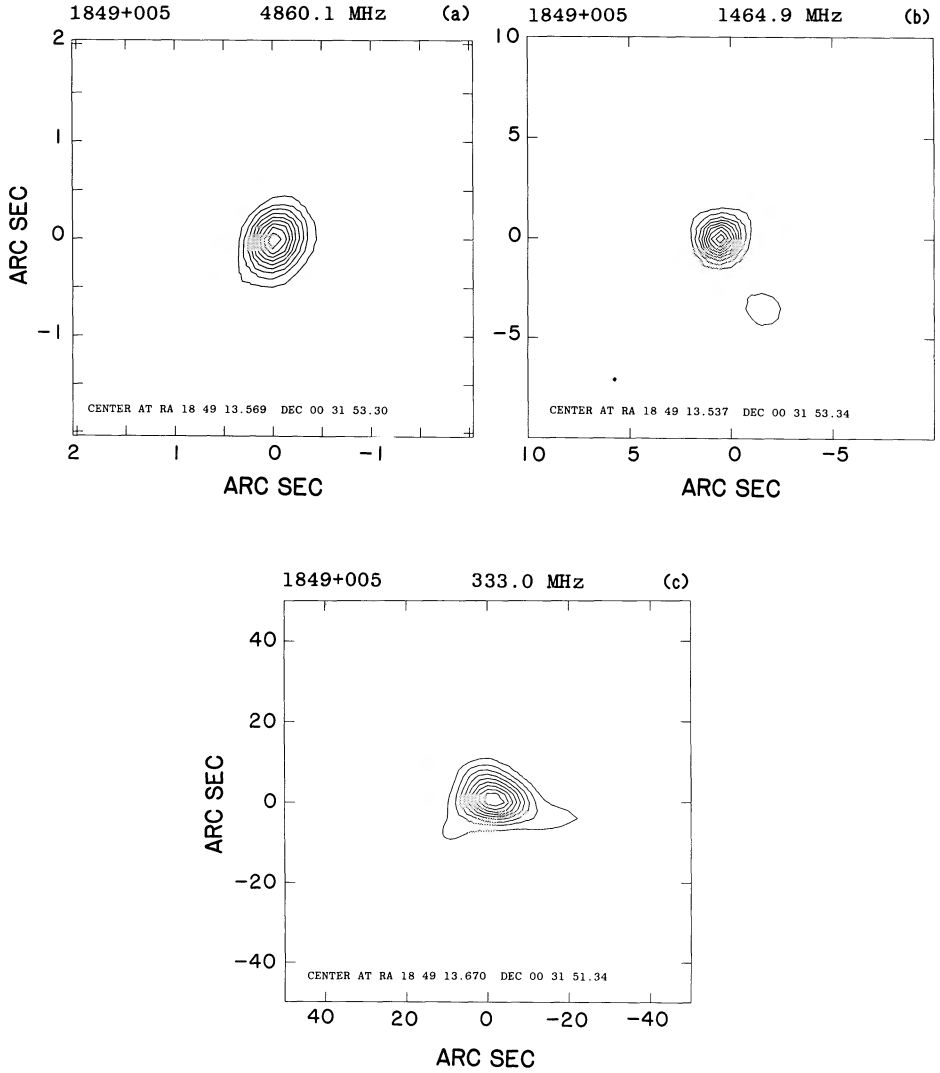

FIG. 4.—VLA images of the compact source 1849+005 at (*a*) 4860 MHz, (*b*) 1465 MHz, and (*c*) 333 MHz. Contours are at −90, −80, −70, −60, −50, −40, −30, −20, −10, −5, 10, 20, 30, 40, 50, 60, 70, 80, and 90% of the peak intensities which are (*a*) 0.550, (*b*) 0.570, and (*c*) 0.919 Jy beam^{-1}. The angular resolution is 0.″5 at 4860 MHz, 1.″5 at 1465 MHz, and 10″ × 6″ in P.A. −75° at 333 MHz.

correction for residual delay and rate, the 2 s correlator records were coherently averaged to 120 s, edited, and then calibrated in the standard manner. Calibration of 2050+364 was facilitated with source models from Phillips & Mutel (1981) for the 1.66 GHz data and from Mutel, Hodges, & Phillips (1985) for the 4.99 GHz data.

The calibrated visibility data were fitted with Gaussian models to obtain estimates of source angular size and zero-spacing flux densities. Error estimates on these quantities are from scatter in the data as determined by the least-squares fitting routine. Upper limits to angular size, where listed, were determined by adding 1 σ to the least-squares fitted value of the zero spacing flux density and then fitting the visibility data for angular size with this value of the flux density held constant.

5. VLBI OBSERVATIONAL RESULTS

In this section we describe the results of our VLBI observations. Of the 62 sources observed, fringes were found for only nine sources. One possible reason for the small number of detections is the relative weakness of the sources in our list. Another more interesting possibility is that some of the sources not detected were so heavily broadened that they were completely resolved even on the shortest baselines. Support for this latter suggestion can be obtained from the survey results of Garwood et al. (1988) who estimate that ~110 of the sources in their survey with flux density greater than 50 mJy are extragalactic. Approximately 50 of the 62 sources we observed are in this category. In the absence of scattering we would have expected to detect more of these sources if they are extragalactic.

Listed in Table 4 are the single-component Gaussian models fitted to our visibility data for the nine sources detected. Column (1) gives the source name, and column (2) lists the frequency of observation. The results of the model fitting are contained in columns (3) and (4), which list, respectively, the zero spacing flux density and the angular size, in milliarcseconds, of the fitted circular Gaussian models at each of the observing frequencies. The quoted errors refer to 1 σ deviation as determined by the least-squares fitting algorithm from

TABLE 3

ADDITIONAL GALACTIC PLANE SOURCES OBSERVED WITH VLBI

Source (1)	R.A. (1950) (2)	Decl. (1950) (3)	l (4)	b (5)	Notes (6)
1908+09B	$19^h08^m36^s.590$	09°13′36″.55	43°.438	−0°.063	
1908+09C	19 08 54.746	09 17 13.45	43.526	−0.101	
1911+108	19 11 06.254	10 48 26.86	45.123	0.133	a
1911+110	19 11 59.976	11 03 58.25	45.454	0.060	a
1912+11A	19 12 14.693	11 19 25.00	45.710	0.127	
1912+11B	19 12 17.112	11 18 26.96	45.700	0.111	
1912+11C	19 12 33.749	11 40 38.60	46.059	0.224	
1912+11D	19 12 36.564	11 42 17.03	46.088	0.227	
1913+115	19 13 19.493	11 33 02.77	46.035	0.000	
1920+149	19 20 16.334	14 55 44.36	49.811	0.107	
1922+155	19 22 23.158	15 34 43.21	50.625	−0.031	b
1929+186	19 29 27.132	18 41 42.86	54.169	−0.009	
1932+204	19 32 59.544	20 25 14.30	56.082	0.105	b
1933+209	19 33 52.354	20 55 07.79	56.617	0.171	
1934+207	19 34 37.428	20 44 50.32	56.554	−0.067	b
1938+22A	19 38 42.122	22 59 03.84	58.966	0.220	
1938+22B	19 38 47.059	22 58 44.26	58.971	0.201	
1948+269	19 48 45.461	26 58 54.30	63.567	0.277	
1951+277	19 51 42.734	27 45 09.76	64.565	0.113	
1954+282	19 54 43.685	28 12 52.70	65.307	−0.214	b,c
1957+299	19 57 53.844	29 58 40.73	67.170	0.127	
2001+304	20 01 30.329	30 25 59.23	67.971	−0.289	b
2008+33A	20 08 14.419	33 22 22.76	71.216	0.108	
2008+33B	20 08 21.082	33 20 50.39	71.207	0.074	
2008+33C	20 08 34.786	33 17 33.76	71.188	0.004	
2008+33D	20 08 52.982	33 13 15.89	71.163	−0.088	b
2009+332	20 09 00.106	33 17 42.50	71.238	−0.068	
2009+333	20 09 00.962	33 18 13.50	71.247	−0.066	
2009+336	20 09 53.568	33 37 27.73	71.615	−0.041	
2010+335	20 10 02.563	33 31 11.96	71.546	−0.125	
2018+363	20 18 39.742	36 22 24.42	74.898	0.019	
2022+374	20 22 03.266	37 28 25.46	76.188	0.097	
2027+383	20 27 02.710	38 22 44.72	77.498	−0.173	b
2031+398	20 31 13.913	39 50 07.19	79.152	0.039	
2033+406	20 33 27.842	40 39 18.58	80.063	0.191	

[a] Identified by Garwood et al. 1988 to be within 2′.4 of a recombination line source.
[b] VLBI fringes found.
[c] Not listed in Garwood et al. 1988.

TABLE 4

GAUSSIAN MODEL FITS TO GALACTIC PLANE VLBI SOURCES

Source (1)	Frequency (GHz) (2)	Flux Density (Jy) (3)	Angular Size FWHM (mas) (4)
1855+031	1.66	0.74 ± 0.26	75.0 ± 7.1
	4.99	0.54 ± 0.14	9.7 ± 1.4
1902+067	4.99	0.09 ± 0.04	4.2 ± 2.4
1922+155	0.61	0.35 ± 0.03	45.3 ± 14.3
	1.66	0.51 ± 0.06	9.5 ± 2.4
	4.99	0.31 ± 0.06	1.3 ± 0.5
1932+204	0.61	0.22 ± 0.01	35.7 ± 12.7
	1.66	0.35 ± 0.03	6.2 ± 1.6
	4.99	0.18 ± 0.02	≤1.8
1934+207	1.66	0.08 ± 0.02	≤3.1
1954+282	0.61	0.76 ± 0.02	22.3 ± 5.4
	1.66	0.58 ± 0.13	3.3 ± 1.0
	4.99	0.42 ± 0.07	≤2.6
2001+304	0.61	0.18 ± 0.02	≤45
	1.66	0.31 ± 0.03	4.5 ± 0.3
	4.99	0.24 ± 0.03	≤0.9
2008+33D	0.61	1.2	361 ± 55
	1.66	1.18 ± 0.70	31.7 ± 15.5
	4.99	1.20 ± 0.18	5.5 ± 0.7
2027+383	1.66	0.44	62.0 ± 6.0

scatter in the visibility data. Table 4 immediately reveals that two of the sources (1855+031 and 2008+33D) have angular sizes which are substantially greater than other sources with flat spectra (as discussed by Fey, Spangler, & Mutel 1989) and which lie far from the Galactic plane. Pearson & Readhead (1981) find 5 GHz angular sizes of several mas for a number of presumably unscattered extragalactic sources at higher latitudes ($b \geq 10°$). In the absence of scattering, the angular size of a flat spectrum, compact extragalactic synchrotron source should scale roughly as the inverse of the observing frequency (Marscher 1977). An unscattered extragalactic source with a 5 GHz angular size of 1 mas would then have a 1.66 GHz angular size of ~3 mas. This angular size is considerably smaller than the sizes we observe at this frequency for 1855+031 and 2008+33D. Our interpretation is that these two sources have observed structures dominated by interstellar scattering. The remaining sources may be affected by interstellar scattering but interpretation of the results is not as straightforward. We now discuss each source separately.

5.1. *1855+031*

At 4.99 GHz figures were found only on the NRAO–VLA, OVRO–HCRK, and OVRO–VLA baselines. Figure 5 shows the visibility data for this source. As can be seen this source is heavily resolved even at 4.99 GHz. A single-component circu-

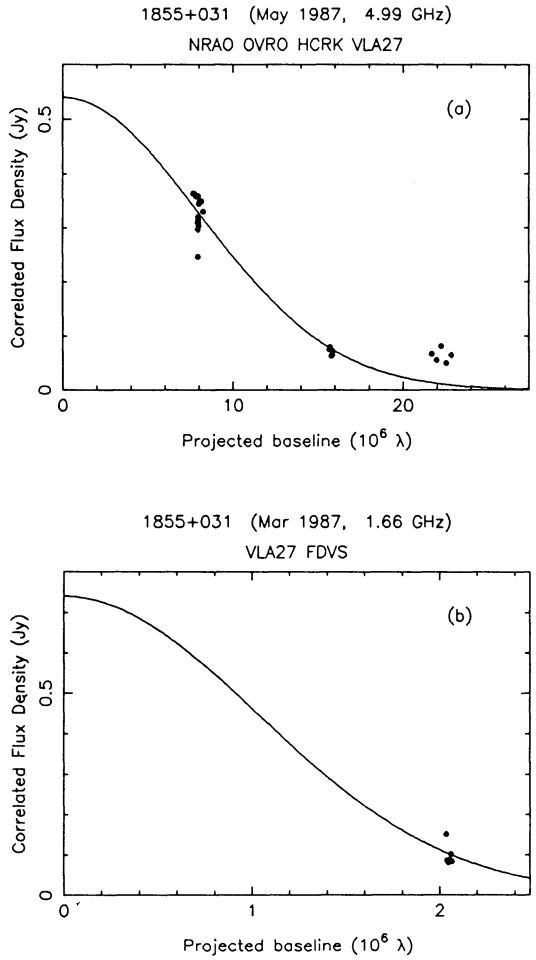

FIG. 5.—Visibility data for the source 1855+031. The data are for (*a*) 4.99 GHz and (*b*) 1.66 GHz. The solid curves represent circular Gaussian models fitted to the visibility data.

lar Gaussian model fitted to the 4.99 GHz visibility data gives an angular size $\theta_{\rm FWHM} = 9.7 \pm 1.4$ mas. Since the source was detected on only the short VLA–FDVS baseline at 1.66 GHz, we need estimates of the zero-spacing flux density to constrain the model fitting. Since this source was also observed with the VLA, we have the zero-spacing flux density that we need. Using an average of the VLA flux density value and the Garwood et al. (1988) value, we arrive at a fitted angular size $\theta_{\rm FWHM} = 75.0 \pm 7.1$ mas. This angular size is considerably larger than would be expected in the absence of scattering. This source was not detected at 0.61 GHz, apparently because it was so heavily broadened that it was completely resolved even on the shortest baselines. Scaling the 1.66 GHz angular size as λ^2 gives an angular diameter of ≈ 550 mas at 0.61 GHz. A source with this angular diameter would have a visibility of $\sim 2\%$ at $0.4 \times 10^6 \lambda$, the shortest projected baseline in the 0.61 GHz VLBI array. The VLBI observations, when taken with the VLA observations, are consistent with a source angular size which is proportional to λ^2.

5.2. *1902+067*

This source was detected only at 4.99 GHz and only on the NRAO–VLA, OVRO–HCRK, OVRO–VLA, and HCRK–VLA baselines. The visibility data for this source are shown in Figure 6*a*. The best circular Gaussian fitted to the 4.99 GHz visibility data gives an angular size $\theta_{\rm FWHM} = 4.2 \pm 2.4$ mas. Because an angular size measurement is available at only this one frequency, we can do no more than set an upper limit to scattering. The 4.99 GHz size, when scaled as λ^2 to 1465 MHz, is consistent with the VLA upper limit of 320 mas.

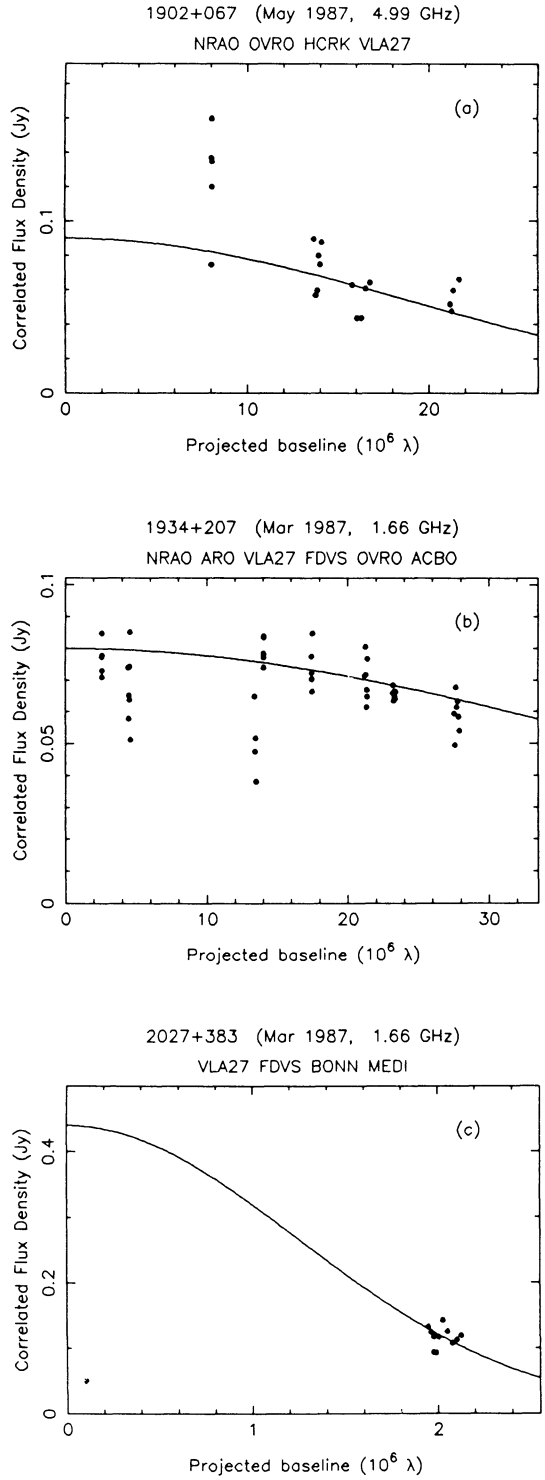

FIG. 6.—Visibility data for the sources (*a*) 1902+067 at 4.99 GHz, (*b*) 1934+207 at 1.66 GHz, and (*c*) 2027+383 at 1.66 GHz. The solid curves represent circular Gaussian models fitted to the visibility data.

5.3. *1922+155*

The structure of this source may be affected by interstellar scattering. The visibility data are shown in Figure 7. The 4.99 GHz visibility data can be represented by a circular Gaussian model with angular size $\theta_{\rm FWHM} = 1.3 \pm 0.5$ mas. The best-fit circular Gaussian to the 1.66 GHz visibility data gives an angular size $\theta_{\rm FWHM} = 9.5 \pm 2.4$ mas. At 0.61 GHz the source is barely resolved and can be represented by a circular Gaussian of angular size $\theta_{\rm FWHM} = 45.3 \pm 14.3$ mas. These measurements indicate that the angular size of this source increases faster with increasing wavelength than would be expected in the absence of scattering (i.e., proportional to λ^2). However, the 4.99 GHz angular size is in no way anomalous for a compact extragalactic source in the absence of scattering (see Pearson & Readhead 1981). If scattering is present, it must be manifested only at the longer wavelengths. In view of the limited amount of data we use these measurements only to set an upper limit to scattering along this line of sight.

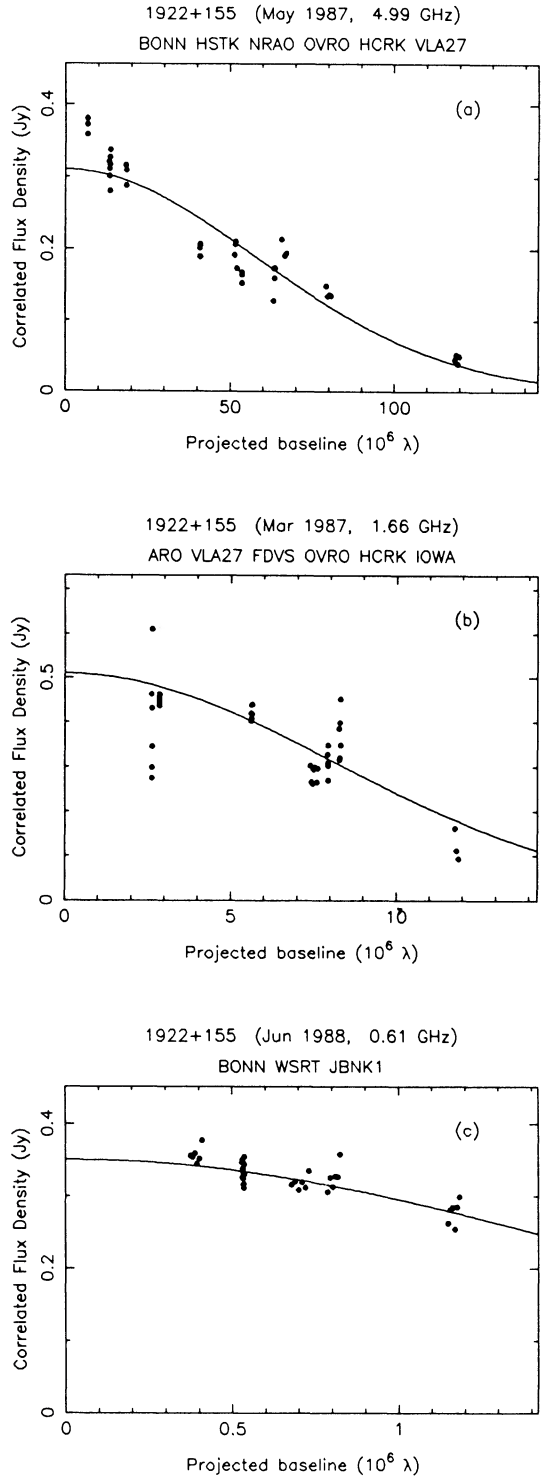

FIG. 7.—Visibility data for the source 1922+155. The data are for (*a*) 4.99 GHz, (*b*) 1.66 GHz, and (*c*) 0.61 GHz. Solid curves represent circular Gaussian models fitted to the visibility data.

5.4. *1932+204*

It is possible that scattering affects the structure of this source, but only at the longer wavelengths. The visibility data are shown in Figure 8. The data indicate that the source is just barely resolved at 4.99 GHz. The best circular Gaussian fitted to the 4.99 GHz visibility data gives an angular size $\theta_{\rm FWHM} = 1.3$ mas. This model is not well constrained, so we set an upper limit to the angular size $\theta_{\rm FWHM} \leq 1.8$ mas. At 1.66 GHz the source is well resolved with a best-fit circular Gaussian angular diameter $\theta_{\rm FWHM} = 6.2 \pm 1.6$ mas. At 0.61 GHz the source is barely resolved. The visibility data are best represented by a circular Gaussian with angular size 35.7 ± 12.7 mas. As with 1922+155, the 4.99 and 1.66 GHz angular sizes are not unusual for such a source. However, the 0.61 GHz size is larger than would be expected in the absence of scattering. Again, we use these measurements only as an upper limit to scattering.

5.5. *1934+207*

This source was detected only at 1.66 GHz and is barely resolved. The visibility data are shown in Figure 6*b*. Because of the weakness of this source, we believe the only reason it was detected was because of the increased sensitivity afforded by the participation of ARECIBO in the observations. The best-fit circular Gaussian to the visibility data gives an angular size of 1.9 mas. The model is not well constrained so we set an upper limit to the angular size $\theta_{\rm FWHM} \leq 3.1$ mas. We use this value to set an upper limit to scattering in this direction.

5.6. *1954+282*

The structure of this source may be affected by interstellar scattering, but only at longer wavelengths. The visibility data for this source are shown in Figure 9. The scatter in the 4.99 GHz visibility data on longer baselines is probably due to intrinsic structure. A circular Gaussian fitted to the 4.99 GHz visibility data yields an angular size $\theta_{\rm FWHM} = 1.7$ mas. Because of the scatter on longer baselines the fitted angular size is not well constrained so we set an upper limit to the 4.99 GHz angular size of 2.6 mas. At 1.66 GHz the source is heavily resolved. The visibility data can be represented by a circular Gaussian with angular size $\theta_{\rm FWHM} = 3.3 \pm 1.0$ mas. Again we see what appears to be intrinsic structure in the 1.66 GHz visibility data. This source is also heavily resolved at 0.61 GHz. A circular Gaussian model fitted to the 0.61 GHz visibility data yields an angular size of $\theta_{\rm FWHM} = 22.3 \pm 5.4$ mas. The angular size of this source between 1.66 and 0.61 GHz is consistent with a λ^2 dependence. However, as with several of the sources discussed above, the 4.99 and 1.66 GHz angular sizes are not unusual for a compact extragalatic source in the

absence of scattering. We use these measurements only to obtain an upper limit to scattering.

5.7. *2001+304*

The structure of this source may be affected by interstellar scattering. The visibility data for this source are shown in Figure 10. As can be seen, the source is unresolved at 4.99 GHz. From the scatter in the visibility data we estimate an upper limit to the angular size of 0.9 mas. At 1.66 GHz the source is heavily resolved. The visibility data are best represented by a circular Gaussian model with angular size $\theta_{\rm FWHM} = 4.5 \pm 0.3$ mas. At 0.61 GHz the source is just barely resolved and has a best-fit angular size of 29.0 mas. The model is not well constrained so we set a generous upper limit to the

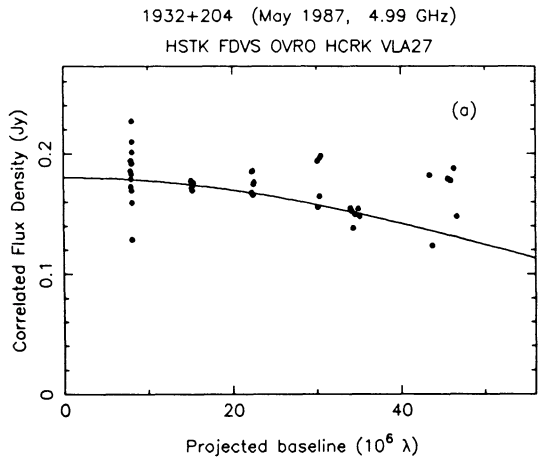

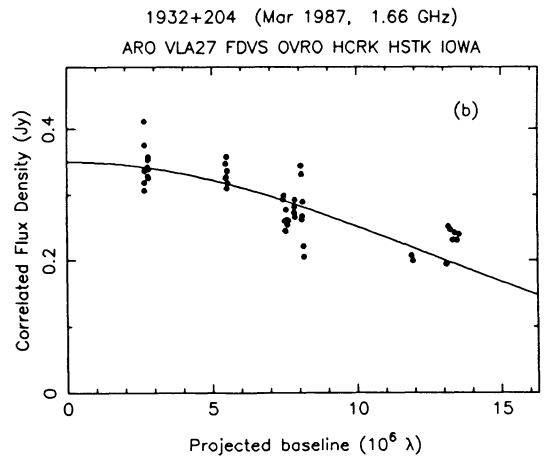

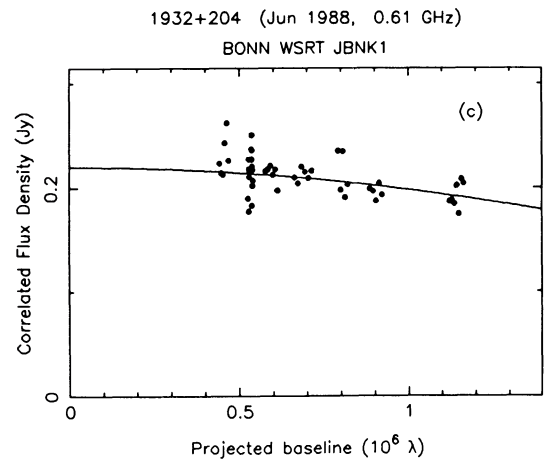

FIG. 8.—Same as Fig. 7, except for the source 1932+204

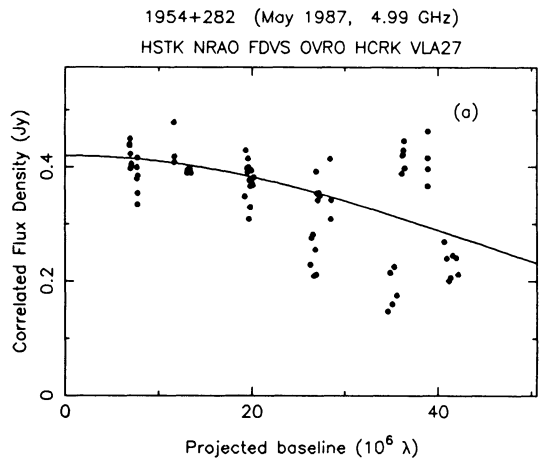

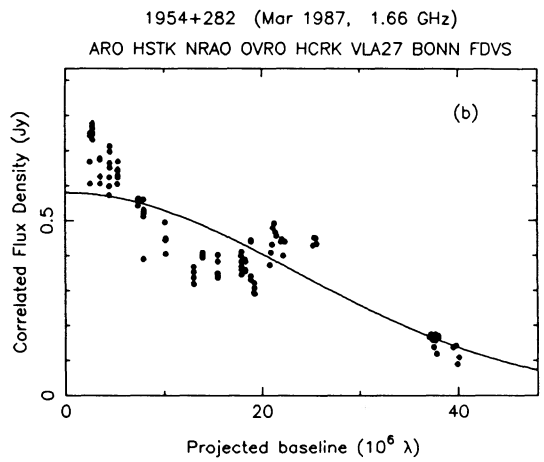

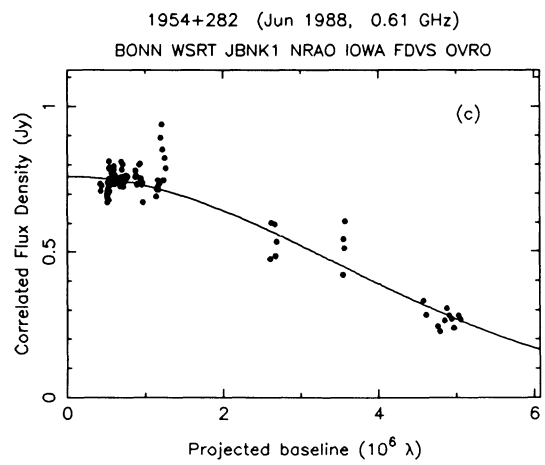

FIG. 9.—Same as Fig. 7, except for the source 1954+282

0.61 GHz angular size $\theta_{\rm FWHM} \leq 45$ mas. If we scale the 1.66 GHz angular size to both 0.61 and 4.99 GHz as λ^2 we find that the measured upper limits at these frequencies are consistent with angular broadening. However, the 1.66 GHz angular size is not unusual for a compact extragalactic source in the absence of scattering so we use the 1.66 GHz angular size only to set an upper limit to scattering.

5.8. *2008+33D*

The visibility data for this source are shown in Figure 11. Even at 4.99 GHz the source is heavily resolved. The 4.99 GHz visibility data can be represented by a circular Gaussian of angular size 5.5 ± 0.7 mas. At 1.66 GHz the source was detected only on the VLA–FDVS baseline, again indicating heavy resolution. Since this source was observed during two

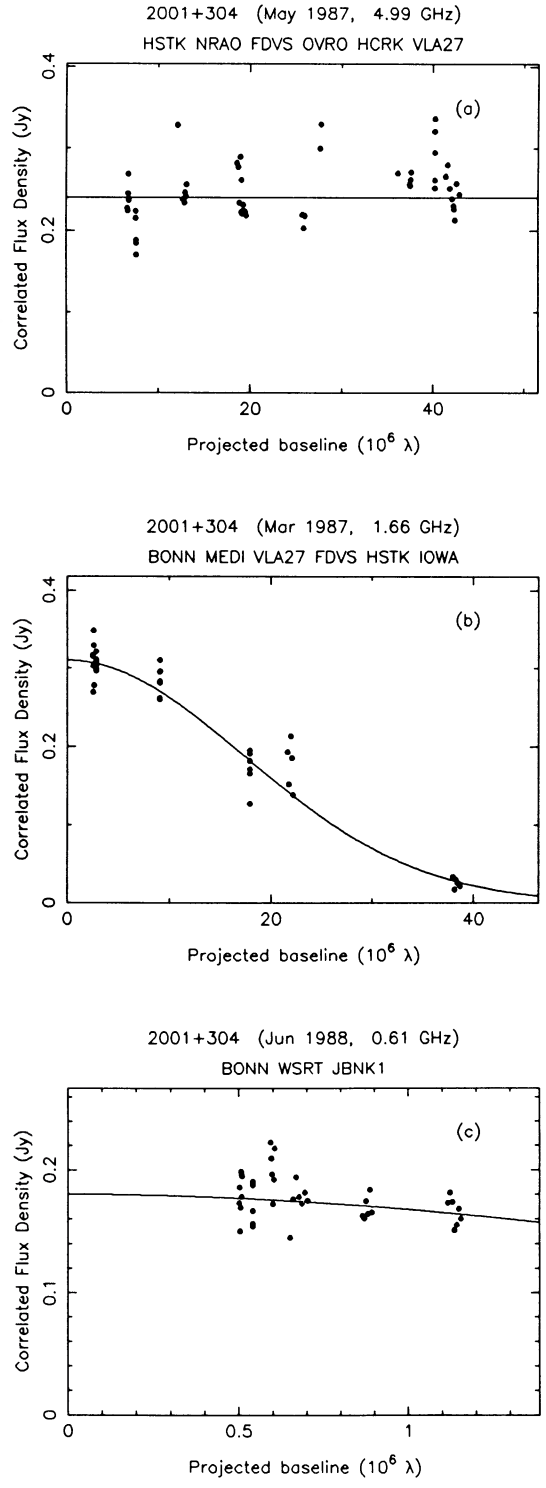

FIG. 10.—Same as Fig. 7, except for the source 2001 + 304

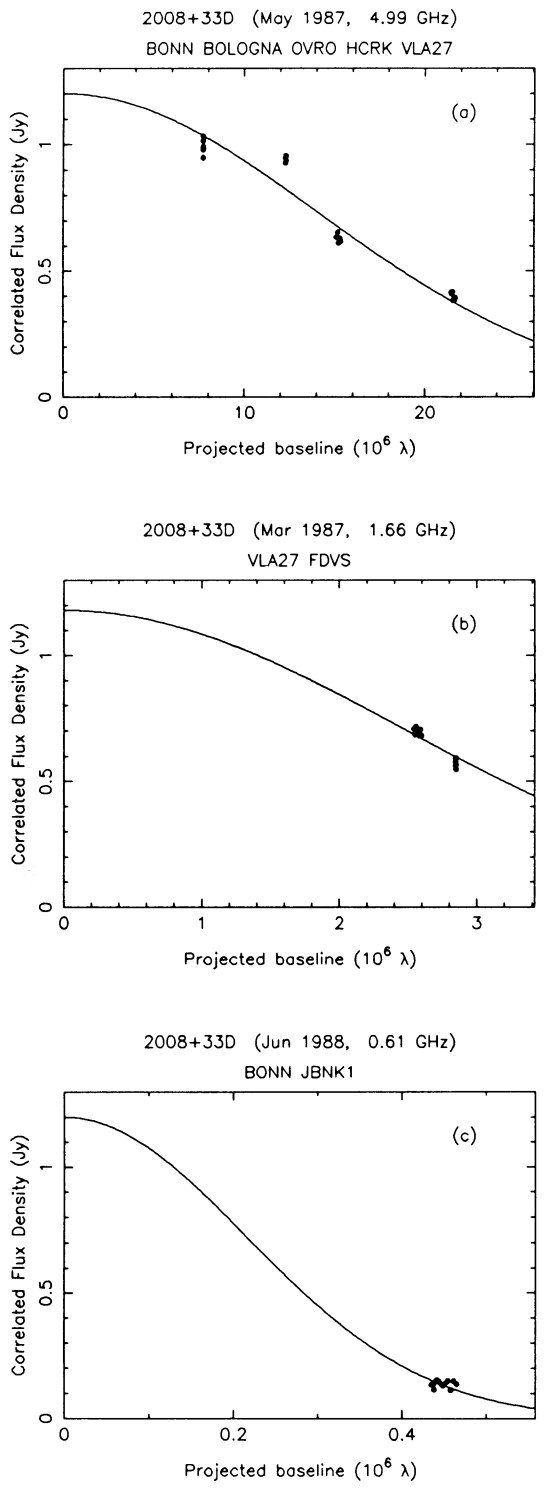

FIG. 11.—Same as Fig. 7, except for the source 2008 + 33D

scans widely separated in hour angle and marginally separated in projected baseline length, it was possible to fit the visibility data with a circular Gaussian model. The result of the model fitting gives an angular size $\theta_{\rm FWHM} = 31.7 \pm 15.5$ mas. At 0.61 GHz the source is so heavily resolved that it was detected during only one scan and only on the very short BONN–JODRELL baseline. Since the source appears to have a flat spectrum, we adopt the 4.99 GHz flux density value for the 0.61 GHz flux density. A circular Gaussian model fitted to the 0.61 GHz visibility data with the flux constrained to the 4.99 GHz value, yields an angular size of 361 ± 55 mas. The angular size of this source shows a λ^2 dependence.

5.9. *2027+383*

This source was detected only at 1.66 GHz and only on the VLA–FDVS baseline during one scan and only on the BONN–BOLOGNA baseline during a second scan. The visibility data for this source are shown in Figure 6*c*. The detection appears to be real because both scans give approximately the same visibility amplitude at about the same projected baseline length. We adopt a value of 0.44 Jy (Garwood et al. 1988) for the 1.66 GHz zero-spacing flux density. With this value held constant, a least-squares fit of a circular Gaussian to the visibility data gives an angular size $\theta_{\rm FWHM} = 62.0 \pm 6.0$ mas, a value larger than would be expected in the absence of scattering. This result indicates that the structure of this source may be dominated by interstellar scattering. However, since the source was detected at only one frequency, we can use this measurement only to set an upper limit to scattering.

6. DETERMINATION OF THE SCATTERING ANGULAR SIZE

In this section we analyze our data and attempt to extract information about the amount of scattering occurring along different lines of sight. The observed structure of a scattered source is a convolution of the intrinsic structure with a scattering function. A broadened source will have a measured angular size that scales with frequency as (Rickett 1977)

$$\theta_{\rm scattered} \propto \nu^{\gamma}, \quad \gamma = -\frac{\alpha}{(\alpha - 2)}, \tag{1}$$

where α is the index of the assumed power-law power spectrum of the turbulent electron density fluctuations. For $\alpha = 11/3$ (the Kolmogorov value), the scattered angular size scales as $\nu^{-2.2}$.

The data we present consist of measurements made using different instruments, each of which is sensitive to different angular scales. Consequently, the VLA and VLBI observations will be discussed separately. The source 1849+005 deserves special consideration and will also be discussed separately.

6.1. *Sources Observed with the VLA*

If the sources listed in Table 2 are to be used as estimators of the total amount of scattering occurring along these lines of sight through the Galaxy, then we must be confident that these sources are extragalactic. We make several arguments for the extragalactic nature of these objects. From our VLA images we note that most of these sources have structurally simple or compact emission with no indication of what might be considered intrinsic structure. In contrast, a number of our images show structure characteristic of H II regions or supernova remnants. For example, the sources 1844−021 and 1849+000 shown in Figures 1*g* and 1*i*, respectively, exhibit extended, asymmetric shell structure. Examination of the 5 GHz continuum maps of Altenhoff et al. (1978) reveals that the sources listed in Table 2 lie well away from any extended continuum emission which could be associated with Galactic objects such as H II regions or supernova remnants. We have also calculated the 1465 MHz brightness temperature for each of these sources using the flux density and angular size measurements listed in Table 2. The results of these calculations reveal that all of these sources have 1465 MHz brightness temperatures in excess of that expected for a thermal continuum source, e.g., $T_B \geq 10^4$ K. We also point out that only one of the 16 sources listed in Table 2 (1832−078) has a position near a recombination line source (see col. [6] of Table 1). This strengthens our argument that the sources listed in Table 2 are extragalactic, since the two sources mentioned above (1844−021 and 1849+000) and others like them do have positions near recombination line sources. Garwood et al. (1988) estimate, from source count arguments, that sources which fall in this category have a high probability of being associated with a Galactic recombination line source. In the case of 1832−078, the source has a 1465 MHz brightness temperature in excess of 2×10^4 K, arguing against the radiation being thermal emission from an H II region.

Finally, the flux density spectral indices ($S_\nu \propto \nu^\alpha$) of the sources with multifrequency detections (1852+021, 1855+031, 1858+05B, 1901+058, and 1905+079) are −0.38, −0.32, −0.48, −0.74, and −0.59, respectively, typical of extragalactic synchrotron sources. The source 1849+005 has a relatively flat spectrum. We conclude that the sources listed in Table 2 have a high probability of being extragalactic and using them for measurements of the amount of scattering occurring along these lines of sight is valid.

Nine of the sources listed in Table 2 (1832−078, 1835−065, 1835−060, 1836−060, 1851+012, 1854+02B, 1854+026, 1902+067, and 1906+083) have measurements only at 1465 MHz. One source (1908+087) was detected only at 333 MHz. To obtain an upper limit to the amount of scattering occurring along the lines of sight to these sources we assume that scattering dominates their observed structure. We scale the angular diameters of these sources to a fiducial frequency of 1 GHz according to the relationship given by equation (1) with a value of $\gamma = -2.2$. These sources thus define upper limits to the scattering occurring along these lines of sight. Our scattering measurements and upper limits from both VLA and VLBI observations are collected in Table 5. Column (1) lists the source name. Column (2) gives the value of the index γ and values of $\theta_{1\ \rm GHz}$ in mas are listed in column (3). Values of γ and $\theta_{1\ \rm GHz}$ were obtained from a least-squares fit when data at three frequencies were available. When data at only a single frequency were available, we assumed $\gamma = -2.2$. The scattered angular size listed in Table 5 for the source 1902+067 is from our VLBI observations. We have also included in this table values for three Galactic plane sources (1829−106, 1922+138, and 1932+174) scaled from 408 MHz VLBI observations of Dennison et al. (1984).

The remaining six sources listed in Table 2 (1849+005, 1852+021, 1855+031, 1858+05B, 1901+058, and 1905+079) have multifrequency detections. The source 1849+005 will be discussed in the next section. The source 1855+031 will be discussed with the VLBI observations. The three sources 1852+021, 1858+05B, and 1901+058 were again used to calculate upper limits to scattering. As an estimate of the scattering contribution to the measured angular size, which will be most pronounced at lower frequencies, we

TABLE 5

GALACTIC PLANE SCATTERED ANGULAR SIZE

Source (1)	Index γ (2)	Angular Size $\theta_{1\ \mathrm{GHz}}$ (mas) (3)
1829−106[a]	≈−2.2	≥48.7
1832−078	≈−2.2	≤4660
1835−065	≈−2.2	≤1950
1835−060	≈−2.2	≤3340
1836−060	≈−2.2	≤3820
1849+005	−1.65 ± 0.12	1120 ± 110
1851+012	≈−2.2	≤3430
1852+021	≈−2.2	≤307
1854+02B	≈−2.2	≤2340
1854+026	≈−2.2	≤1110
1855+031	−1.85 ± 0.06	191 ± 13
1858+05B	≈−2.2	≤368
1901+058	≈−2.2	≤143
1902+067	≈−2.2	≤143
1905+079	−1.68 ± 0.19	≤680
1906+083	≈−2.2	≤2290
1908+087	≈−2.2	≤514
1922+138[a]	≈−2.2	≥32.0
1922+155	−1.67 ± 0.19	≤20.7
1932+174[a]	≈−2.2	≤9.7
1932+204	−1.78 ± 0.57	≤14.0
1934+207	≈−2.2	≤9.6
1954+282	−1.93 ± 0.55	≤8.3
2001+304	≈−2.2	≤13.6
2008+33D	−1.99 ± 0.08	130 ± 13
2027+383	≈−2.2	≤189

[a] Dennison et al. 1984.

scale the 333 MHz angular size of these sources to a fiducial frequency of 1 GHz by a $\lambda^{2.2}$ dependence and list these values in Table 5 as upper limits of $\theta_{1\ \mathrm{GHz}}$. Finally, using the angular size estimates for 1905+079 listed in Table 2, we arrive at a 1 GHz scattering size of 0.″68 ± 0.″06 and index $\gamma = -1.68 \pm 0.19$. These values are listed in Table 5. The structure of this source may be affected by interstellar scattering, but because of the limited amount of information available we list $\theta_{1\ \mathrm{GHz}}$ only as an upper limit.

6.2. *1849+005*

One of the main objectives of our VLA observations was to determine whether the structure of this source is affected by interstellar scattering. A least-squares fit of equation (1) to the angular sizes listed in Table 2 gives values of the index $\gamma = -1.65 \pm 0.12$ and $\theta_{1\ \mathrm{GHz}} = 1.''12 \pm 0.''11$. These values are listed in Table 5.

In Figure 12*a* we have plotted the observed angular size against observing frequency for this source. The solid curve represents an angular size described by equation (1) with values of the index γ and angular size $\theta_{1\ \mathrm{GHz}}$ given above. Inspection of this figure indicates that the measured angular size does not increase as fast as would be expected if the source structure were dominated by scattering but increases faster than would be expected if scattering were not present. The extragalactic nature of this object is indicated by its compactness, variability (Ryle et al. 1978), and flat spectrum. Figure 12*b* shows the flux density spectrum of 1849+005 between 333 MHz and 15 GHz. We have plotted our measured flux density values along with values from Table 2 of Caswell, Milne, & Wellington (1981) and from Table IV of Seaquist & Gilmore (1982). The 408 MHz value is from Dennison et al. (1984). Figure 12*b* shows the flat spectrum nature of 1849+005 at frequencies between 1.4 and 15 GHz, and also indicates the variability of the source. As can be seen from our measurements, the flux density of this source appears to be in a low state.

At lower frequencies the spectrum steepens as indicated by our 333 MHz flux density measurement and the 408 MHz measurement of Dennison et al. (1984). The flux density spectral index ($S_\nu \propto \nu^\alpha$) between 333 and 1465 MHz is −0.73. This steepening of the spectrum at lower frequencies indicates the possible presence of an extended halo or jet. The 1465 MHz map of Seaquist & Gilmore (1982) shows weak extended emission around the position of 1849+005. It is possible that the observed increase in angular size is partly attributable to this extended component rather than scattering. However, in the absence of scattering, we would have expected the high-frequency VLBI observations of Spangler et al. (1986) to have

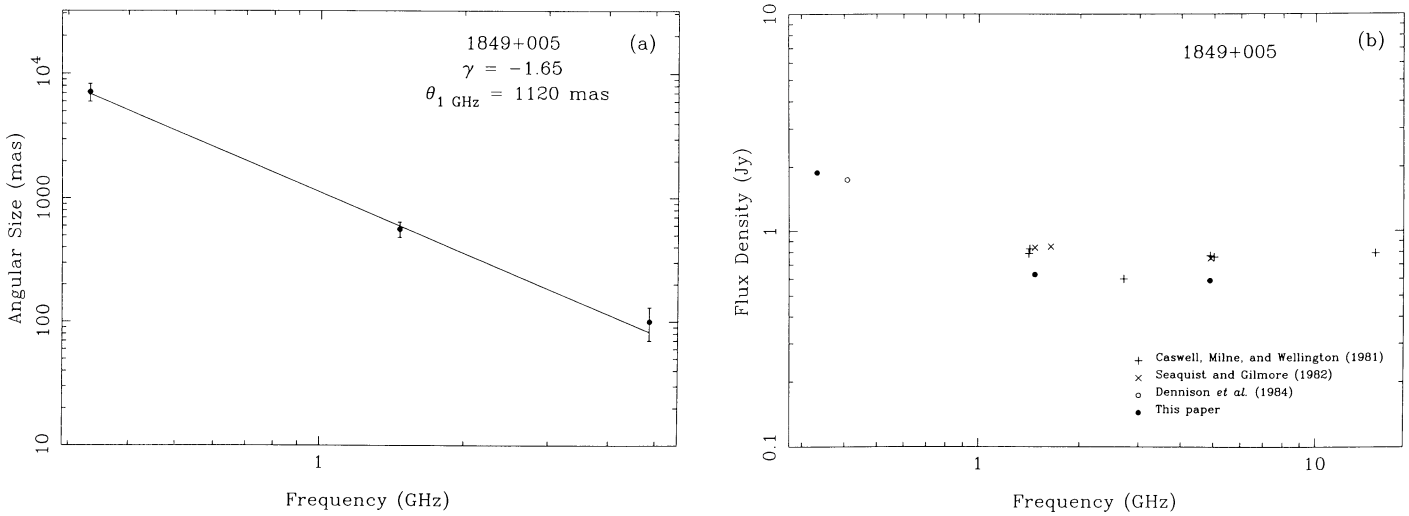

FIG. 12.—(*a*) Angular size vs. observing frequency for 1849+005. The solid curve represents an angular size roughly proportional to the inverse square of the observing frequency, a result expected for angular broadening. (*b*) Flux density versus observing frequency for 1849+005. Values at 333, 1465, and 4860 MHz are from this paper. The 408 MHz measurement is from Dennison et al. (1984). The remaining points are from Caswell, Milne, & Wellington (1981) and Seaquist & Gilmore (1982). This figure illustrates the flat spectrum and variability of 1849+005.

detected the compact core of such an object. The authors failed to detect fringes for this source in any experiment and concluded that, if their null result was due to scattering, the implied 1 GHz broadening size was in excess of 0".35. Their result argues in favor of scattering dominating the structure of this source.

The highly scattered pulsar PSR 1849+00 (Clifton et al. 1988) lies within 10' of 1849+005. From the pulse-broadening measurement of PSR 1849+00, Frail & Clifton (1989) estimate that the angular size due to scattering is ≈0".5 at 1 GHz. Their result is approximately consistent with the amount of scattering calculated from our angular size measurements for 1849+005, and confirms the presence of heavy scattering in this region of the sky. We conclude that the observed structure of 1849+005 is due primarily to scattering occurring along the line of sight to this source, although we cannot rule out a contribution from intrinsic structure. This source appears to be one of the most heavily scattered objects known. There are only two other lines of sight which show equally strong scattering: the Galactic center source, Sgr A, for which Lo et al. (1981) find a λ^2 dependence between 1 and 20 cm with a 1 GHz angular size of ~1".3, and a source seen through NGC 6334 (Rodríguez, Cantó, & Moran 1982) which has $\theta_{1\ \mathrm{GHz}} \approx 8''$.

6.3. *Sources Observed with VLBI*

Of the nine sources detected with VLBI, two (1855+031 and 2008+33D) have structures that appear to be dominated by interstellar scattering and four (1922+155, 1932+204, 1954+282, and 2001+304) have structures which may be affected by scattering. The remaining three sources (1902+067, 1934+207, and 2027+383) were detected at only one frequency and can only be used to set upper limits to scattering.

The calculated values of $\theta_{1\ \mathrm{GHz}}$ and γ for the sources 1855+031, 1922+155, 1932+204, 1954+282, and 2008+33D are listed in Table 5. The source 2001+304 is unresolved at both 0.61 and 4.99 GHz so we scale the 1.66 GHz angular size as $\lambda^{2.2}$ and obtain $\theta_{1\ \mathrm{GHz}} = 13.6$ mas for an upper limit to the scattering. For the four sources whose scattered nature is uncertain, we have listed the values of $\theta_{1\ \mathrm{GHz}}$ as upper limits, even though they probably portray accurate measurements of interstellar scattering. To obtain estimates of the scattering size for 1902+067, 1934+207, and 2027+383 we scale the measured angular size to 1 GHz as $\lambda^{2.2}$ and list these values in Table 5 as upper limits to $\theta_{1\ \mathrm{GHz}}$. We again note that the quoted errors in Table 5 are from scatter in the data as determined from the least-squares fit.

The flux density spectral indices ($S_\nu \propto \nu^\alpha$) of the six sources with multifrequency detections (1855+031, 1922+155, 1932+204, 1954+282, 2001+304, and 2008+33D) are −0.32, −0.06, −0.10, −0.28, 0.13, and 0.00, respectively, indicative of compact extragalactic synchrotron sources. The calculated values of $\theta_{1\ \mathrm{GHz}}$ for the two sources 1855+031 and 2008+33D are larger than would be expected for sources with such spectra.

In Figure 13 we have plotted the observed angular sizes listed in Table 4 against observing frequency for the two scattered sources 1855+031 and 2008+33D. The solid curves for each source represent an angular size described by equation (1) with values of the index γ and angular size $\theta_{1\ \mathrm{GHz}}$ taken from Table 5. Inspection of these plots indicate that the angular sizes of these two sources are in good agreement with that expected from angular broadening. We conclude that the structures of these two sources are dominated by interstellar scattering.

7 INTERPRETATION OF SCATTERING IN THE GALACTIC PLANE

7.1. *Galactic Distribution of Scattering*

The main result of this paper is shown in Figure 14*a* as a plot of scattering size, $\theta_{1\ \mathrm{GHz}}$, versus Galactic longitude. Different symbols distinguish measurements, upper or lower limits, and method of measurement (VLA or VLBI) as indicated by the key. We have also included in this figure results from the Cygnus region observations of Fey, Spangler, & Mutel (1989) and values for three sources scaled from 408 MHz VLBI observations of Dennison et al. (1984). The solid curve in this figure represents results from a model calculation of a "smooth" component of turbulence and will be discussed below. The positions of the sources in Galactic coordinates are shown in Figure 14*b*.

Examination of Figure 14*a* reveals several important results.

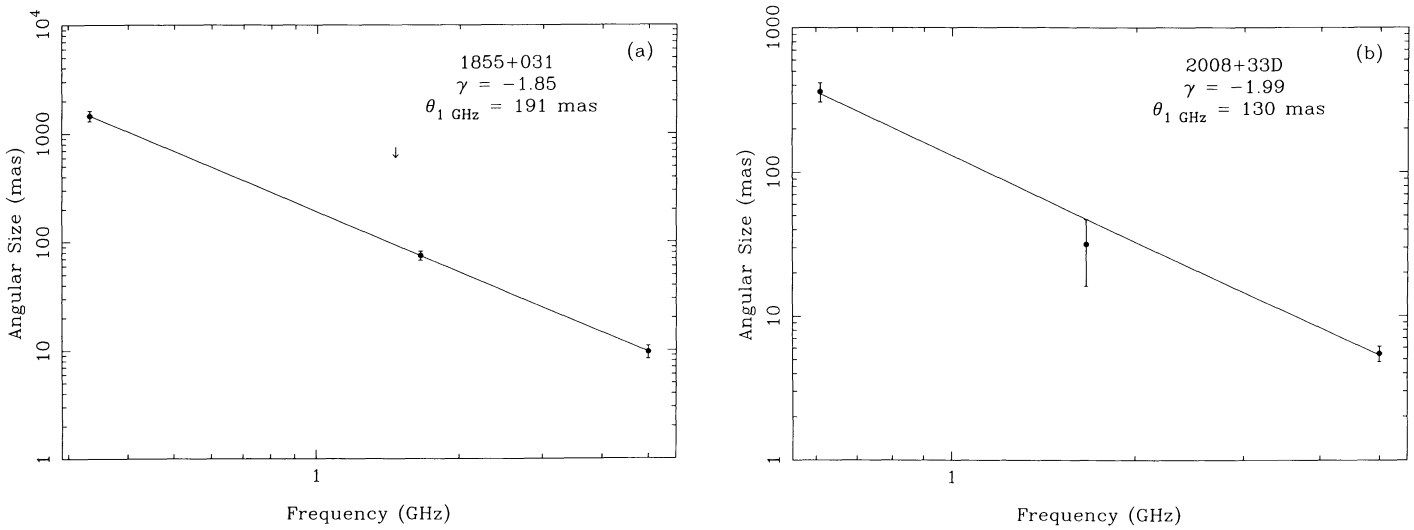

FIG. 13.—Angular size vs. observing frequency for (*a*) 1855+031 and (*b*) 2008+33D. The solid curves represent an angular size roughly proportional to the inverse square of the observing frequency, a result expected for angular broadening. The arrow in (*a*) indicates an upper limit.

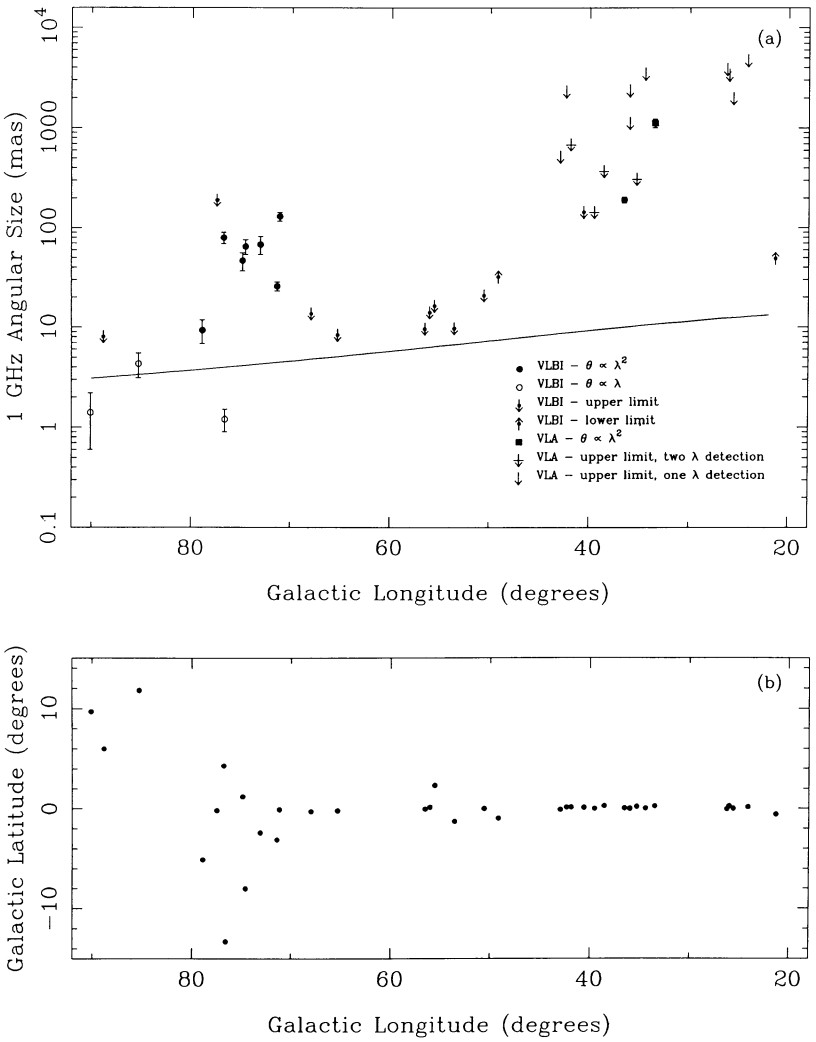

FIG. 14.—(*a*) Scattered angular size vs. galactic longitude. Different symbols indicate measurements, upper limits, or lower limits to the scattered angular size as defined by the key. We have also included in this figure Cygnus region measurements from Fey, Spangler, & Mutel (1989) and values for three sources from Dennison et al. (1984). The solid line represents a model in which the distribution of a "smooth" component of interstellar turbulence (Cordes, Weisberg, & Boriakoff 1985) is exponential in height above the galactic plane and Gaussian in galactocentric radius. (*b*) Distribution of sources in galactic coordinates.

First, there is an overall two-to-three order of magnitude decrease in the scattered angular size between $l = 20°$ and $l = 50°$, with large variations between close lines of sight. In particular, note the change between the sources 1855+031 and 1849+005 (see Table 5). Lines of sight in this longitude range are coincident with the distribution of H II regions in the inner Galaxy, which is known to peak in the galactocentric radius range 4–8 kpc. We also note that although the four data points with $l < 30°$ are shown as upper limits, as was discussed in § 3, we believe that they may portray accurate measurements of interstellar scattering.

Second, there is a relative minimum in the amount of scattering between longitudes of 50° and 70°. We interpret this minimum in the scattering as due to the line of sight passing between spiral arms. Inspection of the 820 MHz map of Berkhuijsen (1972) indicates a minimum in the continuum emission in this same longitude range. This minimum is seen more clearly in Figure 2 of Berkhuijsen (1971) which is a plot of 820 MHz brightness temperature as a function of Galactic longitude at $b = 0°$. The minimum is interpreted by the author as an interarm region bordered by the Sagittarius spiral arm at $l \approx 51°$ and the Carina-Cygnus spiral arm (Bochkarev & Sitnik 1985) at $l \approx 75°$.

Finally, enhanced scattering again becomes prominent in the Cygnus region between longitudes of 70° and 80°. The Cygnus region observations are discussed by Fey, Spangler, & Mutel (1989).

With the exception of the Cygnus region, these results are consistent with those of Alurkar, Slee, & Bobra (1986) who concluded from pulsar scattering measurements that the distribution of turbulence peaks toward the Galactic center. Scattering in the Cygnus region appears to be more like that occurring at low longitudes in that the scattering is enhanced and shows large variations between close lines of sight. In the next sections we address several questions as to the nature of the observed scattering.

7.2. *Comparison with the Uniform Distribution of Turbulence*

In this section we investigate the possibility that a "smooth" component of interstellar turbulence (Cordes, Weisberg, & Boriakoff 1985) can account for at least part of the observed scattering. As is usual, we adopt a power law for the turbulent

electron density power spectrum of the form

$$P_{\delta n_e} = C_N^2 q^{-\alpha}, \quad q_0 \leq q \leq q_1, \tag{2}$$

where C_N^2 is a normalization constant and q_0 and q_1 are spatial wavenumbers corresponding to the outer and inner scales of the turbulence, respectively. We are interested primarily in the variation in the coefficient C_N^2 along different lines of sight. We define a scattering measure as the line of sight integral of the power spectrum normalization constant

$$\mathrm{SM} = \int_0^L C_N^2(s) ds, \tag{3}$$

where L is the path length through the scattering medium.

Scattered angular diameters may be inverted as (Spangler, Fey, & Cordes 1987; Cordes et al. 1988)

$$\mathrm{SM} = \left(\frac{\theta_{\mathrm{FWHM}}}{\theta_0}\right)^{5/3} \nu^{11/3} \ (\mathrm{m}^{-20/3}\ \mathrm{kpc}) \tag{4}$$

where ν is in GHz and $\theta_0 = 130$ mas. Equation (4) holds for extragalactic sources, and we have assumed the Kolmogorov index $\alpha = 11/3$.

We investigate a model for C_N^2 that varies with Galactic radius, r, and height above the Galactic plane, z, as (Cordes et al. 1988)

$$C_N^2 = C_{N_0}^2 e^{-|z|/H} e^{-r^2/A^2}, \tag{5}$$

where $C_{N_0}^2$ is the value at the Galactic center, H is the scale height in z, and A is the galactocentric radial scale length. Substituting equation (5) into equation (3) and integrating (with $L = \infty$ for extragalactic sources) yields the following relationship for scattering measure

$$\mathrm{SM} = \frac{\sqrt{\pi}}{2} C_{N_\odot}^2 \frac{A e^{\beta^2}}{\cos(b)} [1 - \mathrm{erf}(\beta)], \tag{6}$$

where b is Galactic latitude, erf is the standard error function, and $C_{N_\odot}^2$ is the value of C_N^2 at the solar circle. The argument β is defined as

$$\beta = \frac{A \tan(b)}{2H} - \frac{r_{\mathrm{gc}} \cos(l)}{A} \tag{7}$$

where l is Galactic longitude and r_{gc} is the radius of the solar circle. Angular broadening measurements of extragalactic sources have been used to determine values of the scale heights $H = 0.5$ kpc (Cordes et al. 1988) and $A = 7$ kpc (Spangler, Fey, & Cordes 1987; Cordes et al. 1988). From pulsar scattering measurements, Cordes, Weisberg, & Boriakoff (1985) and Cordes et al. (1988) found a value of $C_{N_\odot}^2 = 10^{-3.5}\ \mathrm{m}^{-20/3}$. We adopt these values and calculate the scattering measure as a function of Galactic longitude at $b = 0°$ using equations (6) and (7). Since we are considering scattering only in the Galactic plane, the exact value of the scale height, H, is not important to our results. We set the radius of the solar circle, $r_{\mathrm{gc}} = 10$ kpc. Equation (4) was then used to convert these values to 1 GHz scattered angular size. These calculated values of scattered angular size are plotted as the solid line in Figure 14*a*.

Inspection of Figure 14*a* reveals two things. First, the above model *cannot* account for the falloff of scattering with increasing longitude or the enhanced scattering seen in the Cygnus region. This is not an unexpected result since scattering along these lines of sight is probably due to the interception of several intense "clumps" of turbulence. In the case of the Cygnus region, this assumption is valid since Fey, Spangler, & Mutel (1989) measured factors of 2–5 variation in scattering over angular scales of a few degrees, confirming the existence of a clumped component of interstellar turbulence. Second, the magnitude of scattering predicted by this model is comparable to that observed in the Galactic longitude range $l = 50°$–$70°$, suggesting that scattering in this interarm region may be consistent with a "smooth" component of interstellar turbulence. However, the data of Alurkar, Slee, & Bobra (1986) show that turbulence levels deduced from pulsar scattering in this same longitude range vary by two to three orders of magnitude for lines of sight separated by only a few degrees. Implicit in any measurement of the magnitude of scattering is a knowledge of the path length through the scattering medium. Because pulsars embedded in the scattering material do not sample the entire extent of the scattering medium and due to uncertainties in pulsar distance estimates, comparison of pulsar scattering magnitudes with angular broadening measurements is uncertain. Nevertheless, it is clear from the pulsar data that some, if not all, lines of sight through the interarm region pass through localized regions of intense turbulence.

Our interpretation of these results is that either the number density of clumps or the turbulent intensity of individual clumps along lines of sight in this interarm region is less than for lines of sight passing through spiral arms. This conclusion is consistent with results of a model calculation for the distribution of the "clumped" component of interstellar turbulence presented in § 8 in which it was found that the form of the clump distribution as well as the number density of clumps must change with increasing galactocentric distance. Our results suggest that the majority of the most intense scatterers are probably mainly confined to the spiral arms of the Galaxy, providing further evidence that some Population I object is responsible for regions of enhanced scattering.

7.3. *Comparison with* H166α *Emission Measure*

The basic motivation for a comparison between scattering and H166α emission is a desire to associate enhanced scattering with some known component of the interstellar medium. Previous attempts have so far been unsuccessful. Although heavy scattering was observed in the Cygnus region, Fey, Spangler, & Mutel (1989) were unable to link the enhanced scattering with any particular astronomical object. In particular, no correlation could be found between scattering and H I absorption spectra.

Lockman (1976, 1980) and Anantharamaiah (1986) suggest that normal H II regions are surrounded by tenuous envelopes which are responsible for low-frequency radio recombination lines. Anantharamaiah & Narayan (1988) suggest that if these low-density outer envelopes are turbulent, they may produce the enhanced interstellar scattering of radio sources seen by many observers in the inner Galaxy. Lockman (1980) also suggests that much of the H166α recombination line emission in the inner Galaxy comes from this low-density gas, thus, a comparison between H166α emission and scattering seems a logical endeavor.

We use an H166α recombination line survey in which H166α line temperature measurements were made at $\sim 1°$ intervals in the Galactic plane ($b = 0°$) between Galactic longitudes of 350° and 84°. This survey is an extension of the results reported by Lockman (1976) and is discussed in Lockman (1980). Unpublished portions of this survey were generously made available by the author. The survey was based purely on geometric con-

siderations in that no attempts were made to select directions of discrete continuum sources over directions lacking identifiable continuum emission.

The survey results, given as total line power ($\int T_L\,dv$), reveal that the general trend of the recombination line emission is a decrease of approximately one order of magnitude between longitudes $l = 30°$ and $l = 60°$ (see Fig. 3 of Lockman 1980). In this same longitude range, the scattered angular size decreases by two to three orders of magnitude, qualitatively indicating that scattering decreases faster with increasing Galactic longitude than the recombination line emission.

To facilitate a quantitative comparison with scattering, the total line power measurements were converted to an average emission measure using (Barcia et al. 1985)

$$\mathrm{EM} = 2.25 \times 10^3 T_e^{1.5} n^{-3} b^{-1} \int T_L\,dv\,(\mathrm{cm}^{-6}\ \mathrm{pc}) \qquad (8)$$

where T_e is the electron temperature in Kelvins, n is the principal quantum number (166), b is the departure coefficient (i.e., the ratio of level populations out of local thermodynamic equilibrium to that in local thermodynamic equilibrium), and the total line power is in units of Kelvin times kiloHertz. We assume that stimulated emission makes a negligible contribution to the observed line temperatures. This is a valid assumption only in directions of low continuum intensity. Stimulated emission will tend to increase the observed line intensity and thus lead to an overestimate of the emission measure. We choose an electron temperature of 10^4 K and assume a departure coefficient of $b = 1$. For the assumed electron temperature, $b \geq 0.9$ for the H166α transition for electron densities 10 cm^{-3} or greater (Gordon 1974). To find emission measure values at the longitudes of the program sources, we linearly interpolated values from the recombination line survey. We note, however, that interpolation can overestimate values between lines of sight that have large changes in line emission. Since we are limited by the angular sampling of the survey, we merely make note of this fact and continue.

The interpolated values of emission measure are plotted versus scattered angular size in Figure 15. The plotted symbols are the same as those used in Figure 14*a* to distinguish angular size measurements from upper limits. Only those program sources for which $b \approx 0°$ are included in this figure.

The solid lines in Figure 15 represent the expected dependence of angular size on emission measure if the same gas sampled by the H166α emission is responsible for the observed scattering. The analysis is taken from Spangler & Reynolds (1990) and is as follows. The scattered angular size is given in terms of turbulence properties as (Spangler et al. 1986)

$$\theta_{1\ \mathrm{GHz}} = 8 \times 10^7 \frac{\sigma_n^{1.2}}{L_0^{0.4}} z_{\mathrm{pc}}^{0.6}\ \mathrm{mas} \qquad (9)$$

where σ_n is the rms density fluctuation (cm^{-3}), z_{pc} is the path length through the scattering medium (parsecs), and L_0 is the outer scale of the turbulent electron density power spectrum (centimeters). If we assume that σ_n is related to the electron density by $\sigma_n = \alpha n_e$, where presumably $\alpha \leq 1$, then equation (9) takes on the form

$$\theta_{1\ \mathrm{GHz}} = 8 \times 10^7 \frac{\alpha^{1.2}}{L_0^{0.4}} \mathrm{EM}^{0.6}\ \mathrm{mas} \qquad (10)$$

where $\mathrm{EM} = n_e^2 z_{\mathrm{pc}}$. We thus have a well-defined relationship between scattered angular size and emission measure with the

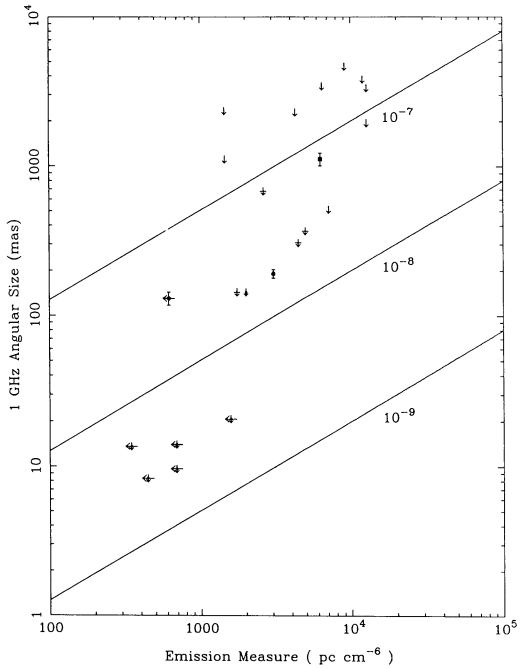

FIG. 15.—Scattered angular size vs. H166α emission measure. Different symbols indicate measurements or upper limits to the angular size as defined by the key in Fig. 14*a*. The solid curves represent the expected dependence of scattered angular size on emission measure if the gas responsible for the H166α emission is the same gas that causes the observed scattering.

coefficient of the relationship, $\alpha^{1.2}/L_0^{0.4}$, giving us the outer scale of the electron density turbulence. We note, however, that this relationship is valid only if the same gas is responsible for both the scattering and the H166α emission. This relationship is plotted in Figure 15 as the solid lines for values of $\alpha^{1.2}/L_0^{0.4} = 10^{-7}, 10^{-8}$, and 10^{-9}.

Although there are insufficient data to perform a rigorous statistical analysis, we believe that this figure indicates that scattering increases *faster* than the H166α data would predict. An equivalent result was obtained by Spangler & Reynolds (1990) who compared scattering measurements in the Cygnus region with emission measures obtained from Hα observations. As was mentioned previously, we believe that the four data points with $l < 30°$ in Figure 14*a* may portray accurate measurements of interstellar scattering. In Figure 15 these are the four data points in the upper right of the figure (EM $> 9 \times 10^3$ pc cm^{-6}). If these points represent actual scattering measurements (rather than upper limits) then the data in this figure do not conform to the relationship given by equation (10). The data would seem to indicate that the scattering size increases as a higher power of the emission measure than 0.6.

This result suggests the possibility that the gas responsible for the H166α recombination line emission is not the same gas responsible for the observed radio wave scattering. Lockman (1980) suggests that at least one component of the H166α recombination line emission in the inner Galaxy comes from a more broadly distributed medium. Our angular broadening measurements are biased in that we have selected sources that lie in directions away from bright, extended continuum sources. We would thus expect that our broadening measurements select against directions of discrete H II regions. From pulsar dispersion measurements, Cordes, Weisberg, & Boriakoff (1985) conclude that large variations of C_N^2 between differ-

ent lines of sight cannot be related to the smooth variations of n_e by a relation $\sigma_n = \alpha n_e$. If a portion of the observed H166α emission arises in a smoothly varying component of the interstellar medium, we would not expect the relationship described by equation (10) to be valid for this component of the interstellar medium. Alternatively, the gas responsible for the H166α recombination line emission could be the same gas responsible for the observed radio wave scattering but with the coefficient $\alpha^{1.2}/L_0^{0.4}$ being a function of emission measure. Spangler and Reynolds (1990) suggest this as an explanation for the observed correlation of radio wave scattering with emission measure in the Cygnus region.

Given the small set of measurements in our data set, interpretation of our results is unclear and leaves open the identification of the regions of enhanced turbulence.

8. GALACTIC DISTRIBUTION OF INTENSE TURBULENT CLUMPS

In this section we develop a statistical model to describe the more intense, "clumped" component of interstellar turbulence (Cordes, Weisberg, & Boriakoff 1985). The model is used to simulate the observed scattering and incorporates randomly located clumps that are subject to the constraint that they obey a specified probability distribution function. We consider a model of this nature so that we may gain some insight into the Galactic distribution of the clumps as well as some of the properties of individual clumps. The model must be capable of reproducing the observed scattering, specifically the magnitude and overall Galactic longitude variation as well as the observed large variations between close lines of sight. In particular, we would like to be able to reproduce the large decline in scattering with increasing longitude, the minimum in the scattering at $l \approx 60°$, and the anomalously high scattering seen in the Cygnus region. We can also use the observations to constrain the scale height of the turbulent clumps, but only for the Cygnus region. We consider first a model intended to describe scattering in the inner Galaxy. The Cygnus region is considered separately. While we make no claims that our analysis gives a unique statistical model for the turbulence, it does provide one description which can be subjected to further observational tests. We feel confident that it presents us with a picture of the gross properties of the clumped scattering medium.

8.1. *The Inner Galaxy*

We consider a model in which the normalized probability distribution function (PDF) for the positions of turbulent clumps is Gaussian in galactocentric radius, r, and exponential in height above the Galactic plane, z. In cylindrical coordinates the distribution is given as

$$p(r, \theta, z) = Ae^{-r^2/a^2} e^{-|z|/h}, \quad (11)$$

where θ is the polar angle, a is the galactocentric radial scale length, h is the z scale height, and A is a normalization constant. We note that this distribution assumes that scattering continues to increase toward the Galactic center. This may not be the case. Our data provide no information about the inner 3 kpc of the Galaxy since we have no measurements for $l \leq 20°$. For this longitude range we can refer to the eight measurements of scattering angle reported by Rao & Slee (1988) for low-latitude ($|b| < 3°$) extragalactic sources observed toward the inner Galaxy ($l < 15°$). The reported scattering angles are comparable with those seen in the Cygnus region and suggest the possibility that the PDF reaches a maximum in the Sagittarius spiral arm, which we observe between $l \approx 20°$–$50°$, and then decreases toward the Galactic center. If this were the case, use of equation (11) would be invalid since this distribution function assumes that scattering continues to increase toward the Galactic center. However, seven of the eight estimates of scattering angle are reported by Rao & Slee (1988) as lower limits, and as such are not inconsistent with the assumption of equation (11). In addition, the much larger pulsar data set of Alurkar, Slee, & Bobra (1986) shows that scattering in the inner Galaxy peaks toward the Galactic center.

To obtain random clump positions, subject to the constraint of equation (11), we use the following integral equation

$$\frac{\int_0^{\xi} p(s)ds}{\int_0^{\infty} p(s)ds} = k_{\xi}, \quad (12)$$

where $p(s)$ is the one-dimensional PDF obtained by integration of the three-dimensional PDF (eq. [11]) over any two of the three coordinate variables, ξ represents the third of the coordinate variables, and k_{ξ} is a random number generated on the interval zero to one. If the integration in equation (12) can be done analytically, then the equation can be inverted to obtain $\xi(k_{\xi})$. We have chosen the form of the PDF (eq. [11]) because of its simplicity and because the integration is analytic. We obtain, for each of the coordinate variables, the following equations

$$r = a\sqrt{-\ln(1-k_r)}, \quad |z| = -h\ln(1-k_z), \quad \theta = 2\pi k_{\theta}, \quad (13)$$

where k_r, k_z, and k_{θ} are random numbers, one for each of the three coordinate variables. Each randomly generated position will represent a "clump" of interstellar turbulence. We point out that these clumps do not necessarily represent objects that may be directly observed (e.g., H II regions or supernova remnants) but may only be regions of enhanced turbulence.

At each of the randomly generated clump positions we assign a local value of C_N^2, the normalization constant of the turbulent electron density power spectrum defined by equation (2), and a clump radius, R_c. Each clump is considered to be uniform so that equation (3) can be used to define a central scattering measure per clump, $\mathrm{SM}_c = 2R_c C_N^2$.

Now that we have defined our distribution, we must compute the number of clumps which lie along a line of sight of interest. The total scattering measure, SM, for a particular line of sight is then the sum of the central scattering measure per clump, SM_c, over all clumps intercepted. In addition, we also include the contribution from the smooth component of interstellar turbulence (eq. [6]). So that we may compare model results with observations, scattering measure is converted to 1 GHz angular size using equation (4).

At low longitudes our data are confined to the Galactic plane so we cannot constrain the z scale height with this model (we will consider the z scale height later when we discuss the Cygnus region). We thus use a value of $h = 100$ pc consistent with the pulsar data of Cordes, Weisberg, & Boriakoff (1985). We present model results in terms of a, N/h, R_c, n_0, and C_N^2. The parameter n_0 is the average number density of clumps defined as $n_0 = N/\pi a^2 h$, where N is the total number of clumps in the distribution. Comparison of model results with observations will be mostly qualitative, involving comparison between model results and the data shown in Figure 14*a*. However, to facilitate a semiquantitative comparison we calculate the mean 1 GHz angular size from our data in the longitude range $l = 33°$–$43°$ and the associated standard deviation. Only

sources with multifrequency measurements are included in this calculation. These same quantities are computed from the model and compared to the observed values which are $\bar{\theta} = 470$ mas and $\sigma_\theta = 370$ mas.

We first consider a simple distribution in which we have a single species of "clump" whose positions are determined by equation (13). Each individual clump has the same radius, R_c, and local value of C_N^2. After many realizations of the model, it became apparent that the only model parameter that is well constrained is the radial scale length. The radial scale length is determined solely by the longitude dependence of the observed scattering. The value of a that adequately reproduced the observed falloff at low longitudes was found to be 3300 ± 300 pc. We are excluding the Cygnus region for the present. The remaining parameters are not at all well constrained. However, a set of parameters was found that could reproduce the observed scattering at low longitudes. It was observed that too small a clump radius resulted in the interception of very few clumps. Increasing the number density of clumps to compensate decreased the variation along different lines of sight to a value which was unacceptable in comparison with the observations. At the other extreme, too large a clump radius resulted in a volume filling factor greater than unity even for a small number density, again drastically reducing variation between different lines of sight. Accordingly, we obtained a compromise value of $R_c \approx 50$ pc.

The model parameters are listed in Table 6 as model 1. Column (1) lists the model number. Subsequent models are discussed below. Columns (2)–(6) give the model parameters, and column (7) lists a ratio which is not used for our first model. As was noted above, we have used a value of $h = 100$ pc for these models. Finally, columns (8) and (9) give the 1 GHz mean angular size and standard deviation as calculated from the model in the longitude range $l = 33°$–$43°$. We hesitate to list ranges for the parameters listed in this table because it is not at all obvious whether these parameters are unique. We merely list sets of parameters capable of reproducing at least part of the observed scattering.

Figure 16*a* shows the predicted scattering from model 1, calculated at 1° intervals in the Galactic plane, superposed on Figure 14*a*. The model curve is the solid line and represents an average over 10 realizations of model 1. Error bars must be multiplied by a factor of $\sqrt{10}$ to reflect the true standard deviation at each point. The base level of the predicted scattering is defined by the contribution from the "smooth" component of interstellar turbulence described earlier. As can be seen, this model predicts the scattering at low longitudes rather well but fails at the higher longitudes. In particular, the model does not predict any scattering for $l \geq 50°$. Also note the overestimate of angular size at $l \approx 50°$. This is a result of the rather large value of C_N^2 of 1000 $m^{-20/3}$ required to produce the strong scattering at low longitudes. With a clump size of 50 pc, passage through one clump results in a 1 GHz scattered angular size of ~ 2000 mas. We point out that the line of sight at $l \approx 50°$ intercepted a clump on only one of the 10 realizations from which the model curve was generated. This results in an average over 10 values, nine of which are zero, thus producing the large error bar and smaller mean value.

We have also used the model to predict scattering along lines of sight to several pulsars. Model values were compared to observed values taken from Alurkar, Slee, & Bobra (1986). The pulsars lie in the longitude range $l = 28°$–$71°$ and have $b \leq 5°$. Each of these pulsars is more than 6 kpc from the Galactic center. To account for the extragalactic scattering data we have used a galactocentric radial scale length $a = 3.3$ kpc. From the distribution function (eq. [11]) we calculate that the probability of a clump being at a radius greater than 6 kpc is only 4%. Thus we would expect, and indeed find, that model 1 cannot account for the pulsar scattering since few if any lines of sight will intercept a clump. If a clump was intercepted in the model, the predicted pulsar scattering was well in excess of that actually observed because of the large value of C_N^2. These considerations demonstrated the need for a more complicated clump distribution model.

In reality, one would not expect the interstellar medium to consist of a single species of "clump" just as we would not expect every H II region in the Galaxy to have the same size. We could imagine a number of more complex models, such as a power law distribution of clump sizes or a scattering strength C_N^2 which depends on Galactic radius, but our data do not warrant consideration of such complex models. We can, however, investigate some of the properties of such models by introducing two species of clumps. This is a crude way of introducing a clump distribution function. We consider a distribution of clumps whose positions are described by equations (13) and again give each clump the same radius. We give the majority of clumps a smaller value of C_N^2 than was used in model 1, and let only a small fraction have the same value as used in model 1. We also use the same radial scale length and clump radius as found for model 1. This model therefore had two additional free parameters in comparison to model 1, the local value of C_N^2 of the less intense clumps and R, the ratio of the number density of the clumps with the larger value of C_N^2 to the number density with the smaller value. Finding the value C_N^2 of the weaker clumps was relatively straightforward because scattering produced by these clumps had to be consistent with the observed scattering at $l \geq 50°$. Experience indicated a favored value of ~ 10 $m^{-20/3}$ and also yielded a value of R of 0.2. The parameters for this model, referred to as model 2, are given in Table 6. We note that the number density of clumps (col. [5]) had to be doubled to compensate for the decreased scattering measure per clump caused by the smaller value of C_N^2 of the less turbulent clumps.

Model 2 is shown in Figure 16*b* superposed on Figure 14*a*.

TABLE 6

MODEL PARAMETERS

Model (1)	Scale (pc) (2)	N/h (pc^{-1}) (3)	R_c (pc) (4)	n_0 (10^{-7} pc^{-3}) (5)	C_N^2 ($m^{-20/3}$) (6)	R (7)	$\bar{\theta}$ (mas) (8)	σ_θ (mas) (9)
1	$a = 3300$	20	50	5.85	1000	...	600	530
2	$a = 3300$	40	50	11.7	10, 1000	0.2	320	240
3	$a = 4200$, 3200	40	50	5.05, 3.73	10, 1000	0.3	420	310
Cyg	$h = 50$	8	25	78.4	0.2, 5.0	0.25	...	...

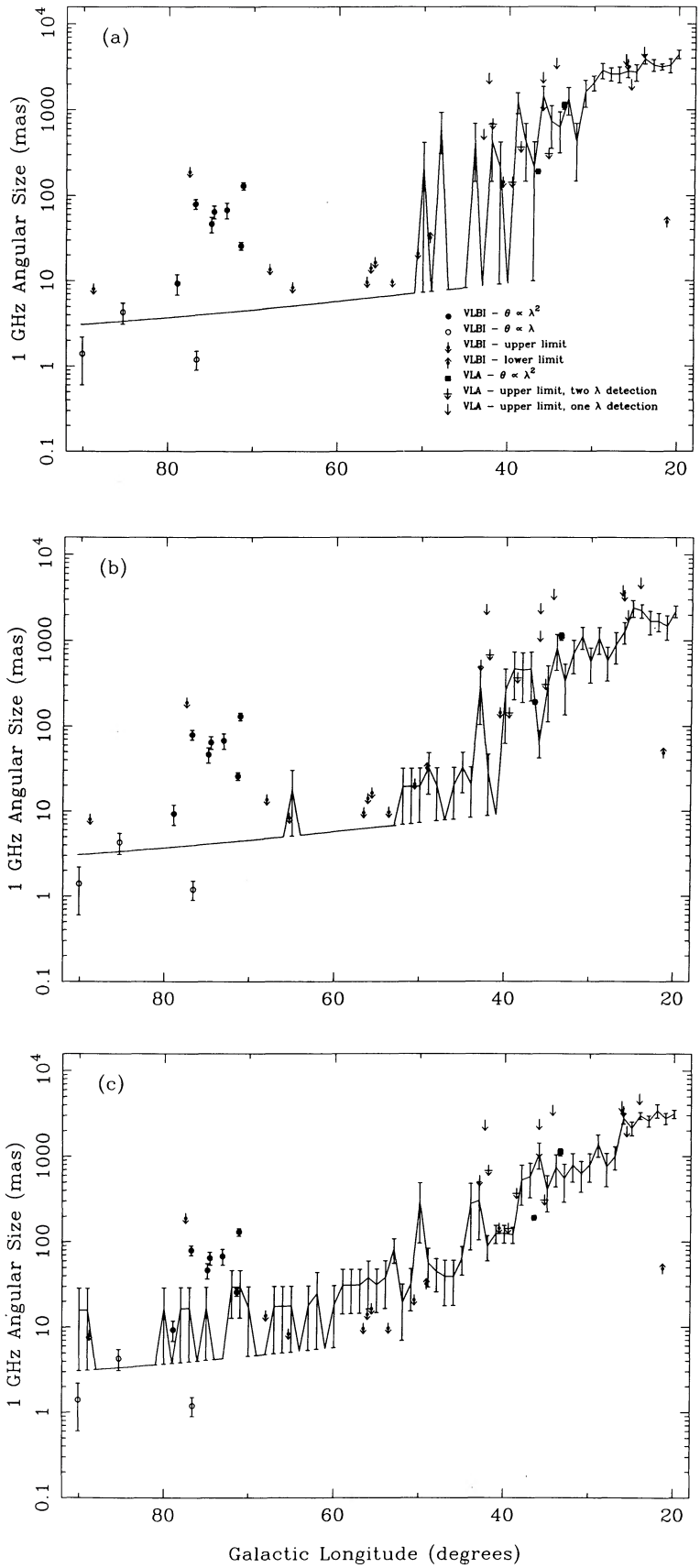

FIG. 16.—Predicted scattering from (*a*) model 1, (*b*) model 2, and (*c*) model 3 for the inner Galaxy. Model results are plotted at 1° intervals in the galactic plane and are superposed on Fig. 14*a*. The model curves are the solid lines and represent an average over 10 realizations. Error bars must be multiplied by a factor of $\sqrt{10}$ to reflect the true standard deviation at each point. The base level of the predicted scattering is defined by the contribution of a "smooth" component of interstellar turbulence described in the text. See Table 6 for a list of model parameters.

This figure shows that model 2 appears to better represent the observed scattering. Although the overall magnitude of the model prediction is low, as evidenced by the lower value of $\bar{\theta}$ given in Table 6, the model does show the necessary line of sight variation and does not overestimate scattering at $l \geq 50°$ for the extragalactic data, or for the pulsar data (not shown). The overall larger number density of clumps increases the number of clumps with Galactic radius 6 kpc or greater. However, there are still an insufficient number of clumps with radius 6 kpc or greater so that very few pulsar lines of sight intercept a clump.

We require a model that is consistent with both the extragalactic data and the pulsar data. The results of model 2 suggests that we use a larger radial scale length to account for pulsar lines of sight. A larger radial scale length will produce a distribution with more clumps at larger galactocentric radii, thus increasing the probability that a pulsar line of sight will intercept a clump. However, model 1 indicates that the radial scale length must be ~ 3300 pc to account for the falloff seen in the extragalactic source data. As a compromise, we again consider a two species distribution whose positions are described by equation (13), but give each species of clump a different radial scale length. To be consistent with the scattering at $l \geq 50°$ the clumps with the smaller value of C_N^2 are given a larger radial scale length than the more intense clumps. We constrain these values of C_N^2 to the values used in model 2 and vary only the two radial scale lengths and the ratio of the number of intense to the number of weak turbulent clumps. Parameters for the most satisfactory model are listed in Table 6 as model 3. The radial scale lengths for the weak and intense clumps were found to be 4200 and 3200 pc, respectively. The ratio listed in column (7) was found to be 0.3.

Model 3 is shown in Figure 16*c* superposed on Figure 14*a*. As can be seen in this figure, model 3 does a much better job of representing the extragalactic source data. In addition, over 50% of the pulsar lines of sight intercept at least one clump in the model. The pulsar scattering predicted by the model is consistent with the observations in both the magnitude of the observed scattering and the line of sight variation.

8.2. *The Cygnus Region*

In the previous section we developed a computer simulation to describe the observed scattering in the Galactic plane. The models considered so far have not taken into account the anomalously large scattering seen in the Cygnus region. It is possible that model 3 described above can account for at least part of the observed scattering in this region. As can be seen in Figure 16*c*, model 3 predicts scattering at the longitude of the Cygnus region. However, the predicted scattering is not sufficient in magnitude or variation to explain the more heavily scattered sources. In this section we consider a model specifically designed to account only for the scattering seen in the Cygnus region. Because our observations in the Cygnus region include sources several degrees from the Galactic plane, we may incorporate the scale height of the clumps in our statistical model.

In the case of the Cygnus region we have a good idea of the spatial extent of the region. Bochkarev & Sitnik (1985) discuss observations in the region having Galactic longitude $l = 65°$–$90°$ and Galactic latitude $b \leq 10°$. The authors estimate that the objects which produce the X-ray and optical radiation are located at distances of 0.5 to 2.5 kpc from the Sun. This gives a maximum line of sight distance through the region of ~ 2 kpc. Using the mean distance of 1.5 kpc and the observed angular extent in the Galactic plane of $\sim 25°$, we find that the region has a scale transverse to the line of sight of ~ 650 pc. To model the region, we create a distribution of "clumps" randomly distributed inside an ellipse which lies in the Galactic plane and has major and minor axes of 2000 and 650 pc, respectively. The distribution is located such that a line of sight through the center has a Galactic longitude of $l = 78°$, which is approximately the center of the Cygnus region on the sky. The z coordinates of the distribution are calculated in the same manner as in the previous models described above (see eq. [13]). Although artificial, this distribution may represent the spiral arm nature of this region.

Because of our knowledge of the geometry of the Cygnus region we can proceed to place certain limits on some of the model parameters. For instance, the most heavily scattered source in our sample, 2008+33D, has a 1 GHz angular size of 130 mas. If we assume that the scattering observed for this source was the result of the line of sight traversing one turbulent clump then we can constrain the scattering measure per clump. Using equation (4) we obtain an upper limit to the scattering strength per clump $\mathrm{SM}_c \leq 1\ \mathrm{m}^{-20/3}$ kpc. At the other extreme, the least scattered source, 2050+364 (Mutel & Hodges 1986), has a 1 GHz angular size of ~ 10 mas. Again, if we assume the scattering of this source was the result of one clump, then we can constrain $\mathrm{SM}_c \geq 0.01\ \mathrm{m}^{-20/3}$ kpc. From Fey, Spangler, & Mutel (1989), the two scattered sources with the closest lines of sight (2021+317 and 2023+336) have an angular separation of $\sim 2°$. If we assume the lines of sight to these two sources traverse different clumps and assume that the clumps are at a distance of 2.5 kpc then we can constrain the maximum clump size, $R_c \leq 40$ pc.

With this information we can immediately rule out a distribution with a single species of clump. The argument is as follows. In our model we need a minimum value of $\mathrm{SM}_c \approx 0.01\ \mathrm{m}^{-20/3}$ kpc to account for the least scattered source. If every clump in the distribution has this value, then lines of sight to more heavily scattered sources must traverse multiple clumps. With a value of $R_c \approx 40$ pc this value of SM_c translates to a local value of $C_N^2 \approx 0.13\ \mathrm{m}^{-20/3}$. If this value of C_N^2 were uniform throughout the Cygnus region in our model, then the maximum line of sight of 2000 pc would give a total scattering measure, $\mathrm{SM} \approx 0.26\ \mathrm{m}^{-20/3}$ kpc, which translates into a 1 GHz angular size of ~ 58 mas. Thus a single species of clump, consistent with the least scattered source, cannot account for the most heavily scattered source.

We consider a two species distribution of clumps. Each clump is given the same radius but one of two different values of C_N^2. Model results are presented in terms of h, N/h, R_c, n_0, C_N^2, and R. The parameter R is, as before, the ratio of the number of clumps with the larger value of C_N^2 to the number with the smaller value. The parameter, n_0 is the average number density of clumps defined as $n_0 = N/\pi cdh$, where N is the total number of clumps in the distribution, h is the z scale height, $c = 1000$ pc is the semimajor axis of the elliptical distribution, and $d = 325$ pc is the semiminor axis. To facilitate a semiquantitative comparison of model results with observations we calculate the mean 1 GHz angular size from our data in the range $l = 65°$–$90°$, $|b| \leq 5°$ and the associated standard deviation. These same quantities are computed from the model and compared to the observed values which are $\bar{\theta} = 48$ mas and $\sigma_\theta = 43$ mas.

Since we have scattering measurements out of the plane in

the Cygnus region, we can also use the model to constrain the z scale height. Model values were calculated only for lines of sight to which we have measurements. Model parameters were found by comparing observed values to single realizations of the model. These are $R_c = 25$ pc, $n_0 = 7.84 \times 10^{-6}$ pc^{-3}, $C_N^2 = 0.2$, 5.0 m$^{-20/3}$, and $R = 0.25$. These model parameters are listed in Table 6. As with the previous models, clump radius and number density were obtained by determining which combinations of the two parameters produced the observed line of sight variations. To find the z scale height, average values of $\theta_{1\ \mathrm{GHz}}$ were computed from ten realizations of the model with the above parameters held constant while varying the scale height. Model results were then compared with the observed values. The z scale height found to satisfactorily produce scattering consistent with the observations was $h = 40$–70 pc.

Figure 17 shows the results of this model, which are plots of 1 GHz angular size on the lines of sight probed by the measurements in Fey, Spangler, & Mutel (1989) and this paper. The sizes of the open circles in this figure are directly proportional to 1 GHz angular size. The dotted circle in the lower right corner of each panel represents an angular size of 130 mas. The plus symbols represent sources with an angular size less than 8 mas. The first panel in this figure shows the actual observations. The other panels show model results from three different realizations using the parameters listed above and a value of $h = 50$ pc. The mean angular size and its associated standard deviation are shown in the lower left of each panel. These values are to be compared to the values from the actual observations listed in the lower left of the first panel. Although there are variations between realizations, as can be seen in this figure, the model satisfactorily reproduces the magnitude and spatial variability of the observed scattering.

8.3. *Discussion of Model Results*

We have developed a statistical model to simulate the observed scattering in the Galactic plane. The analysis reveals several significant results. First, the radial scale length of the distribution function indicates that the majority of the intense scatterers are confined to within ~ 3.5 kpc of the Galactic center. In addition, it seems that the distribution function of the clumps must evolve with galactocentric distance. This result is evident not only in the need for different species of clumps with different scale lengths but also in that model results for the Cygnus region are quite different from the results for the inner Galaxy. The Cygnus region seems to have more clumps per pc^{-3} but they are less intense scatterers. As was mentioned above, it is possible that model 3 can account for at

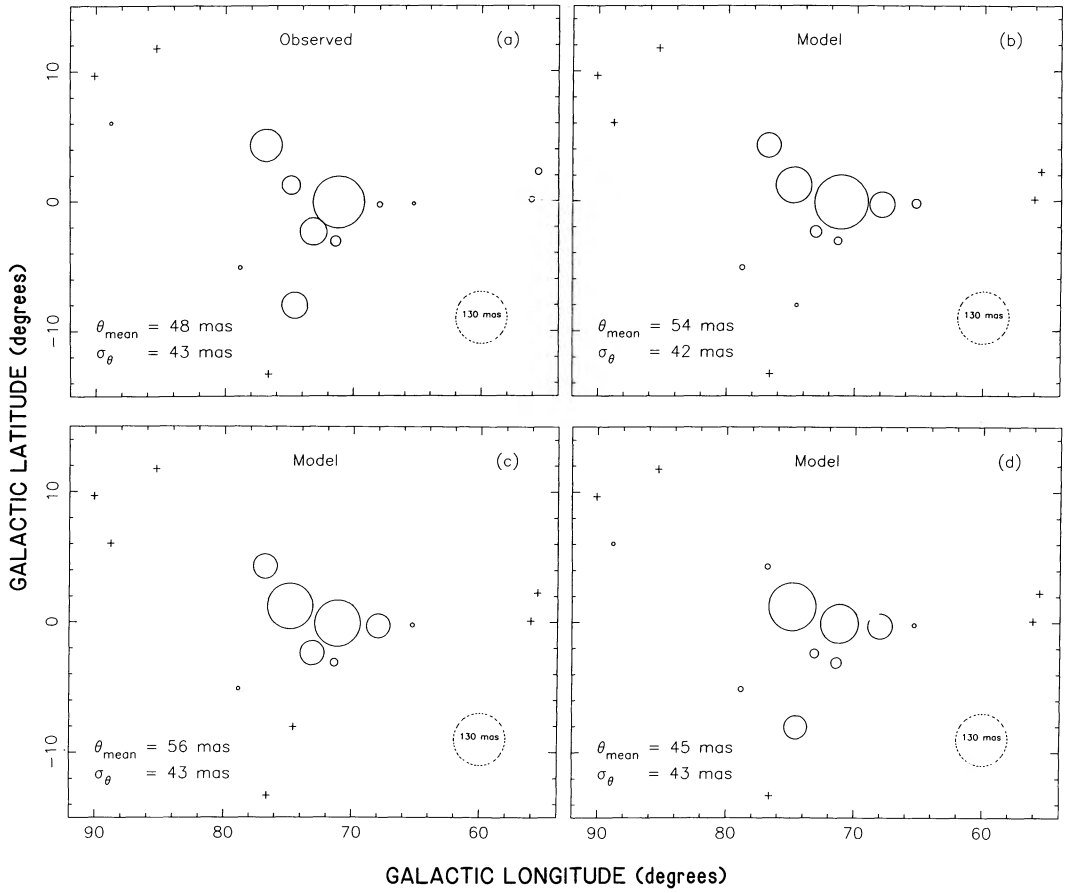

FIG. 17.—Simulated scattering for the Cygnus region. This figure shows the results of the Cygnus model, which are plots of 1 GHz angular size vs. galactic longitude and latitude. The sizes of the open circles in this figure are directly proportional to 1 GHz angular size. The dotted circle in the lower right corner of each panel represents an angular size of 130 mas. The plus symbols represent sources with an angular size less than 8 mas. The first panel in this figure shows the actual scattering measurements from Fey, Spangler, & Mutel (1989) and this paper. The other panels show model results from three different realizations using model parameters listed in Table 6.

least part of the observed scattering in this region, but the predicted scattering is not sufficient to explain the more heavily scattered sources. Perhaps a more complex distribution function, explicitly taking into account spiral arm structure, would be better capable of simulating all of the observed scattering.

Second, the clump sizes found for both models are consistent with the path lengths of 50–200 pc, derived from low frequency recombination line measurements (Anantharamaiah 1985a, b), for the low-density outer envelopes of normal H II regions. They are also consistent with the sizes of H II regions seen in other galaxies for which Courtes (1977) lists a "most frequent diameter" of 80 pc (for M31) or 40 pc (for M33). However, our model predicts electron densities far in excess of those found by Anantharamaiah (1985a, b) for the low-density outer envelopes of normal H II regions. For the inner Galaxy model we found clumps with $C_N^2 = 1000\ \mathrm{m}^{-20/3}$. A value of C_N^2 this large implies extremely turbulent clumps. For the assumed spectrum of equation (2), the total rms electron density for an outer scale, $L = 2\pi/q_0 = L_{\mathrm{pc}}$ is (Cordes et al. 1988)

$$\sigma_n = 0.74(C_N^2)^{1/2} L_{\mathrm{pc}}^{1/3}\ \mathrm{cm}^{-3}\ , \qquad (14)$$

where C_N^2 has units of $\mathrm{m}^{-20/3}$. If we assume the outer scale is on the order of the clump size then our model predicts rms electron densities on the order of 100 cm^{-3}. From pulsar scattering measurements, Cordes, Weisberg, & Boriakoff (1985) find average values of C_N^2 ($\bar{C}_N^2 = SM/D$) ≈ 0.1–$1\ \mathrm{m}^{-20/3}$ for lines of sight longer than a few kpc toward the inner Galaxy. Cordes et al. (1988) estimate that if clumps are of parsec size then local values of C_N^2, which are the values used in our model, are 10^3–10^4 times larger than the average values. Thus, the local value of C_N^2 predicted by our model does not seem unreasonable, at least for lines of sight at low longitudes. But, if we again assume that $\sigma_n = \alpha n_e$ and let $\alpha = 1$, we have $n_e \approx 100$ cm^{-3} which is one to two orders of magnitude larger than the densities found by Anantharamaiah (1985a, b). In addition, electron densities this large imply rather large emission measures. Using a clump radius of 50 pc and the above electron density we calculate an emission measure, $\mathrm{EM} = n_e^2 z_{\mathrm{pc}} = 10^6$ pc cm^{-6}, a value two orders of magnitude larger than the maximum observed emission measure shown in Figure 15. These results could be due to the rather simple nature of our model. A more complex distribution function might not require such large values of C_N^2 to produce the observed scattering. For example, in model 3 only 30% of the clumps in the distribution have this large a value of C_N^2. The majority have a value of $10\ \mathrm{m}^{-20/3}$ which implies a value of $n_e \approx 10\ \mathrm{cm}^{-3}$. This value leads to an emission measure of $\approx 10^4$ pc cm^{-6}, which is within the observed values. In the Cygnus region we also find that we do not need extremely turbulent clumps. Here we calculate values of σ_n of ~ 2 and 8 cm^{-3} for the two species of clumps considered.

Finally, the value of the z scale height in the Cygnus region predicted by our model is entirely consistent with the value $h \leq 100$ pc found by Cordes, Weisberg, & Boriakoff (1985) from pulsar scattering measurements. In addition, the number of clumps in the Cygnus model distribution is within a factor of 4 of the estimated 110 high-luminosity stars in the Cygnus region (Bochkarev & Sitnik 1985). These are the stars capable of producing H II regions.

9. CONCLUSIONS

We have made dual-frequency VLA and multifrequency VLBI observations of a number of sources in the Galactic plane. The observations have been used to estimate the amount of interstellar scattering in the Galactic plane as manifested by angular broadening of the observed sources. Our results constrain the longitude dependence of scattering in the Galactic plane. We have interpreted the results of the observations, reported as measurements of the angular size due to scattering, in terms of a two-component turbulent scattering medium. We have also compared the observed scattering to H166α recombination line emission in an attempt to associate scattering with some known component of the interstellar medium. Our conclusions are as follows:

1. The extragalactic source 1849+005 appears to be broadened to a 1 GHz scattered angular size of $\sim 1\farcs1$. However, we cannot exclude a contribution to the scattered angular size from intrinsic structure.
2. The two sources 1855+031 and 2008+33D have observed structures that are dominated by interstellar scattering.
3. Sources that may be affected by interstellar scattering are 1905+079, 1922+155, 1932+204, 1954+282, and 2001+304. More observations of these sources are needed to confirm or refute the presence of scattering.
4. The observed scattering in the Galactic plane decreases with increasing Galactic longitude reaching a minimum at $l \approx 60°$ and then becomes prominent again in the Cygnus region.
5. The magnitude of scattering in the interarm region between $l = 50°$–$70°$ is comparable to that predicted by a model calculation of a "smooth" component of interstellar turbulence. This result suggests that the more intense "clumps" of interstellar turbulence may be mainly confined to the spiral arms of the Galaxy.
6. Results of a computer simulation designed to investigate the "clumped" component of interstellar turbulence indicates that a complex distribution of clumps is necessary, with a range of scattering strengths, and that the form of the clump distribution as well as the density of clumps must change with increasing galactocentric distance. The simulation constrains the z scale height in the Cygnus region to be ~ 40–70 pc.
7. Although there is a weak correlation between scattering and H166α emission measure, interpretation of this result is unclear and leaves open the identification of the regions of enhanced turbulence.

This work was supported at NRL by an award from the National Research Council, at the University of Iowa by grants NAGW-806 and 831 from the National Aeronautics and Space Administration, and at Cornell University by the Alfred P. Sloan Foundation, NSF grant AST-8520530, and the National Astronomy and Ionosphere Center. We sincerely thank R. W. Garwood for providing prepublication positions of Galactic plane sources. In addition, we would like to thank F. J. Lockman who generously made available unpublished portions of an H166α recombination line survey of the Galactic plane. Finally, we thank the US VLBI network and the EVN for their participation in our observations.

REFERENCES

Altenhoff, W. J., Downes, D., Pauls, T., & Schraml, J. 1978, A&AS, 35, 23
Alurkar, S. K., Slee, O. B., & Bobra, A. D. 1986, Australian J. Phys., 39, 433
Anantharamaiah, K. R. 1985a, J. Ap. Astr., 6, 177
———. 1985b, J. Ap. Astr., 6, 203
———. 1986, J. Ap. Astr., 7, 131
Anantharamaiah, K. R., & Narayan, R. 1988, in AIP Conf. Proc. 174, ed. James M. Cordes, Barney, J. Rickett, & Donald C. Backer (New York: AIP), p. 185
Baars, J. W. M., Genzel, R., Pauliny-Toth, I. I. K., & Witzel, A. 1977, A&A, 61, 99
Barcia, A., Gómez-González, J., Lockman, F. J., & Planesas, P. 1985, A&A, 147, 237
Berkhuijsen, E. M. 1971, A&A, 14, 359
———. 1972, A&AS, 5, 263
Bochkarev, N. G., & Sitnik, T. G. 1985, Ap. Space Sci., 108, 237
Caswell, J. L., Milne, D. K., & Wellington, K. J. 1981, MNRAS, 195, 89
Clifton, T. R., Frail, D. A., Kulkarni, S. R., & Weisberg, J. M. 1988, ApJ, 333, 332
Cordes, J. M., Spangler, S. R., Weisberg, J. M., & Clifton, T. R. 1988, in AIP Conf. Proc. 174, ed. James M. Cordes, Barney J. Rickett, & Donald C. Backer (New York: AIP), p. 180
Cordes, J. M., Weisberg, J. M., & Boriakoff, V. 1985, ApJ, 288, 221
Courtes, G. 1977, in Topics in Interstellar Matter, ed. H. van Woerden (Dordrecht: Reidel), p. 209
Dennison, B., Thomas, M., Booth, R. S., Brown, R. L., Broderick, J. J., & Condon, J. J. 1984, A&A, 135, 199
Fey, A. L., Spangler, S. R., & Mutel, R. L. 1989, ApJ, 337, 730
Frail, D. A., & Clifton, T. R. 1989, ApJ, 336, 854
Garwood, R. W., Perley, R. A., Dickey, J. M., & Murray, M. A. 1988, AJ, 96, 1655
Gordon, M. A. 1974, in Galactic and Extra-Galactic Radio Astronomy, ed. G. L. Verschuur & K. I. Kellermann (Berlin: Springer-Verlag), p. 51
Lo, K. Y., Cohen, M. H., Readhead, A. C. S., & Backer, D. C. 1981, ApJ, 249, 504
Lockman, F. J. 1976, ApJ, 209, 429
———. 1980, in Radio Recombination Lines, ed. P. A. Shaver (Dordrecht: Reidel), p. 185
Marscher, A. P. 1977, ApJ, 216, 244
Molnar, L. A., Mutel, R. L., Reid, M. J., & Johnston, K. J. 1991, ApJ, submitted
Moran, J. M., Rodríguez, L. F., Green, B., & Backer, D. C. 1990, ApJ, 348, 147
Mutel, R. L., & Hodges, M. W. 1986, ApJ, 307, 472
Mutel, R. L., Hodges, M. W., & Phillips, R. B. 1985, ApJ, 290, 86
Pearson, T. J., & Readhead, A. C. S. 1981, ApJ, 248, 61
Phillips, R. B., & Mutel, R. L. 1981, ApJ, 244, 19
Rao, A. P., & Slee, O. B. 1988, MNRAS, 234, 853
Rickett, B. J. 1977, ARAA, 15, 479
Rodríguez, L. F., Cantó, J., & Moran, J. M. 1982, ApJ, 255, 103
Ryle, M., Caswell, J. L., Hine, G., & Shakeshaft, J. 1978, Nature, 276, 571
Seaquist, E. R., & Gilmore, W. S. 1982, AJ, 87, 378
Spangler, S. R., Fey, A. L., & Cordes, J. M. 1987, ApJ, 322, 909
Spangler, S. R., Mutel, R. L., Benson, J. M., & Cordes, J. M. 1986, ApJ, 301, 312
Spangler, S. R., & Reynolds, R. J. 1990, ApJ, 360, 116